Additive Manufacturing 36 (2020) 101564

Contents lists available at ScienceDirect

Additive Manufacturing

journal homepage: www.elsevier.com/locate/addma

Reproducibility of sound-absorbing periodic porous materials using additive manufacturing technologies: Round robin study

Tomasz G. Zieliński [a,*], Kamil C. Opiela [a], Piotr Pawłowski [a], Nicolas Dauchez [b], Thomas Boutin [b], John Kennedy [c], Daniel Trimble [c], Henry Rice [c], Bart Van Damme [d], Gwenael Hannema [d], Rafał Wróbel [e], Seok Kim [f], Shahrzad Ghaffari Mosanenzadeh [f], Nicholas X. Fang [f], Jieun Yang [g], Baltazar Briere de La Hosseraye [g], Maarten C.J. Hornikx [g], Edouard Salze [h], Marie-Annick Galland [h], René Boonen [i], Augusto Carvalho de Sousa [i,j], Elke Deckers [i,j], Mathieu Gaborit [k,l], Jean-Philippe Groby [l]

[a] Institute of Fundamental Technological Research, Polish Academy of Sciences, ul. Pawińskiego 5B, 02-106 Warsaw, Poland
[b] Université de Technologie de Compiègne, Alliance Sorbonne Université, CNRS FRE 2012, Laboratoire Roberval, Centre de recherche Royallieu, CS 60319, 60203 Compiègne CEDEX, France
[c] Trinity College Dublin, Department of Mechanical & Manufacturing Engineering, Dublin 2, Ireland
[d] Swiss Federal Laboratories for Materials Science and Technology, Laboratory for Acoustics/Noise Control, Überlandstrasse 129, 8600 Dübendorf, Switzerland
[e] Swiss Federal Laboratories for Materials Science and Technology, Advanced Materials Processing, Überlandstrasse 129, 8600 Dübendorf, Switzerland
[f] Massachusetts Institute of Technology, Department of Mechanical Engineering, 77 Massachusetts Avenue, Cambridge, MA, USA
[g] Eindhoven University of Technology, Department of the Built Environment, P.O. Box 513, 5600 MB Eindhoven, The Netherlands
[h] Ecole Centrale de Lyon, Université de Lyon, CNRS UMR 5509, Laboratoire de Mécanique des Fluides et d'Acoustique, 36 avenue Guy de Collongue, 69134 Écully CEDEX, France
[i] KU Leuven, Department of Mechanical Engineering, Celestijnenlaan 300B box 2420, 3001 Heverlee, Belgium
[j] DMMS-D Lab, Flanders Make, Belgium
[k] KTH Royal Institute of Technology, Department of Aeronautical and Vehicle Engineering, SE-100 44 Stockholm, Sweden
[l] Laboratoire d'Acoustique de l'Université du Mans (LAUM), UMR CNRS 6613, Institut d'Acoustique – Graduate School (IA-GS), CNRS, Le Mans Université, France

ARTICLE INFO

Keywords:
Porous materials
Designed periodicity
Additive manufacturing
Sound absorption

ABSTRACT

The purpose of this work is to check if additive manufacturing technologies are suitable for reproducing porous samples designed for sound absorption. The work is an inter-laboratory test, in which the production of samples and their acoustic measurements are carried out independently by different laboratories, sharing only the same geometry codes describing agreed periodic cellular designs. Different additive manufacturing technologies and equipment are used to make samples. Although most of the results obtained from measurements performed on samples with the same cellular design are very close, it is shown that some discrepancies are due to shape and surface imperfections, or microporosity, induced by the manufacturing process. The proposed periodic cellular designs can be easily reproduced and are suitable for further benchmarking of additive manufacturing techniques for rapid prototyping of acoustic materials and metamaterials.

1. Introduction

Although standard porous materials, like open cell foams or fibrous material, are still very competitive for acoustic treatments, their efficiency is limited in the low frequency range by their thickness [1]. If their microstructure can be optimized to meet specific requirements [2–4], their manufacturing is now achievable using 3D printing techniques for experimental validation at the scale of a laboratory. Indeed, the development of Additive Manufacturing (AM) technologies [5–12] gives new possibilities to manufacture and test optimized micro-geometries. Moreover, new acoustic materials (or their prototypes) are already being developed using AM technologies, e.g.: 3D printed periodic foams [13], optimally graded porous materials [2], adaptable sound absorbers [14], acoustic metamaterials based on the

* Corresponding author.
E-mail address: tzielins@ippt.pan.pl (T.G. Zieliński).

https://doi.org/10.1016/j.addma.2020.101564
Received 29 February 2020; Received in revised form 16 July 2020; Accepted 25 August 2020
Available online 2 September 2020

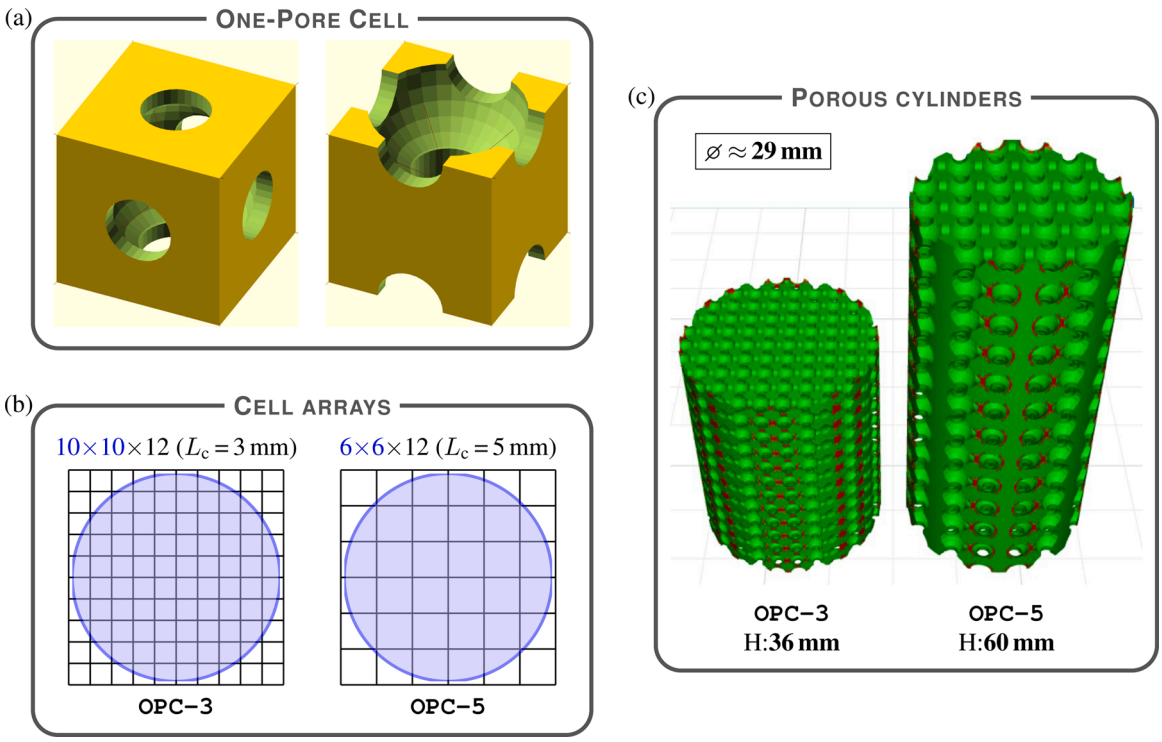

Fig. 1. One-Pore Cell (OPC) geometry: (a) two alternative representations of the periodic cell, (b) arrays of cells (L_c = 3 or 5 mm) for CAD models of samples with a diameter of 29 mm, (c) CAD models of the periodic cylindrical samples OPC-3 and OPC-5 (diameter about 29 mm and height 36 or 60 mm, respectively).

Kelvin cell [15], sound-absorbing micro-lattices [16], metallic phononic crystals for use in water [17], periodic acoustic structures composed of rigid micro-rods [18] or micro-bars [19], and even micro-perforated panels [20,21] and plates with complex patterns of micro-slits [22]. Most of this research indicates great potential for the development of new acoustic materials using AM technology. However, 3D printing technology should be evaluated regarding the quality of the reproduced micro-geometry and its influence on sound dissipation. The purpose of this work is to evaluate the impact of several additive manufacturing technologies on the sound absorption of 3D printed samples. Following well-established traditions in acoustic [23,24] and non-acoustic [25–27] testing of materials, this work is a round robin test, i.e. an inter-laboratory test, where the manufacturing of samples and their acoustical measurements are performed independently by various laboratories. The only thing that is shared at the beginning of such independent investigations is the agreed periodic micro-geometry of the porous materials developed in that way.

The influence of additive manufacturing processes on the sound absorption of a few materials with designed porosity has already been reported [28,29]. The current paper presents most of the results obtained from the measurements of over 90 samples manufactured in six different AM technologies on 16 AM devices (15 different) in six laboratories, and acoustically tested by the sample manufacturers and also in three other laboratories to ensure the correctness of the measurements. For most samples of the same cellular design, good and sometimes very good consistency of the measurement results was obtained, which along with their microscopic examination allows to indicate technologies, materials and devices capable of the best reproduction of the designed porosity. It seems that such comparative acoustic tests can also be used to assess the quality of reproduction of designed materials with fine details. The main purpose of this study is to check the feasibility and accuracy of reproduction of the designed periodic geometry using additive manufacturing, which should serve to prototype samples used for validation of advanced modelling of sound-absorbing porous materials [30] and metamaterials with designed (possibly optimized) periodic geometry efficient in the low and medium audible frequency ranges. The focus is on the attenuation of airborne acoustic waves penetrating porous media with a rigid skeleton. Therefore, the thickness of the walls and ligaments in the proposed porous cellular designs, as well as the rigidity of the materials used for production ensure that poro-elastic effects do not exist or are insignificant. The outline of this paper is as follows. The periodic geometries of the porous samples are described in Section 2. Then, the manufacturing techniques are briefly discussed and samples produced using them are presented in Section 3. The whole scheme of the round robin study, including sample production and acoustic tests in the impedance tube using the transfer function method with two microphones [31–33], is discussed in Section 4. Finally, the measurement results are compared in Section 5.

2. Periodic porosity designs

2.1. One-Pore Cell geometry

Two kinds of cubic cells with periodic porosity were designed for this study. In both cases, the periodic porosities are completely open and consist of spherical pores connected by short cylindrical channels.

The first periodic cell is very simple: it contains a single spherical pore that is connected to identical pores of neighbouring cells through very short (horizontal or vertical) channels of the same size. The pore diameter is $0.9L_c$ and the channel diameter is $0.4L_c$, where L_c is the size (edge length) of the cubic cell. This One-Pore Cell (OPC) is depicted in Fig. 1(a) in two alternative representations: with the pore in the centre of the cube and with the pore shifted vertically from this position by half the size of the cube. The latter version was used to generate two types of a Computer-Aided Design (CAD) geometry for porous cylindrical samples shown in Fig. 1(c). For the first CAD geometry of the cylindrical sample, the cubic cell size was set to L_c = 3 mm, and then a three-dimensional array of 10 × 10 × 12 cells was constructed, see Fig. 1(b), from which a vertical cylinder with a diameter of 29 mm and a height of 36 mm was cut. Cylindrical samples with this periodic cellular design

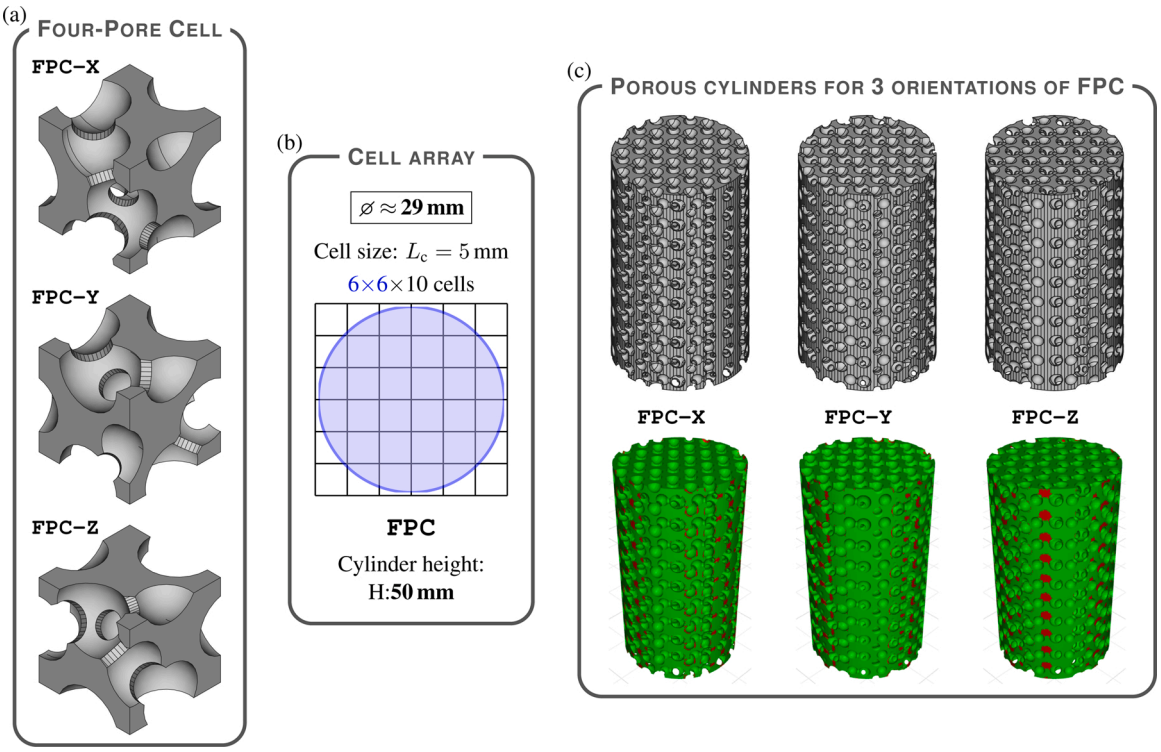

Fig. 2. Four-Pore Cell (FPC) and the geometry for FPC samples (diameter 29 mm and height 50 mm): (a) three orientations of the periodic cell, (b) cell array, (c) CAD models for FPC samples, generated in *FreeCAD* (upper row) and analysed using *Z-SUITE* slicer (lower row).

will be designated as OPC-3 samples. For the second CAD geometry the cubic cell size was set to $L_c = 5$ mm and a vertical cylinder with a diameter of 29 mm was cut from the array of $6 \times 6 \times 12$ such cells so that its height is 60 mm, see Fig. 1(b) and (c). These higher cylindrical samples with larger pores will be designated as OPC-5 samples.

CAD geometry models for OPC-3 and OPC-5 samples with larger diameters are constructed in a similar way, only the cell array must be larger in both horizontal directions, for example, for a diameter of 40 mm the cell array must have $14 \times 14 \times 12$ cells for OPC-3, and (at least) $8 \times 8 \times 12$ cells for OPC-5. If a sample is to be 3D printed with a diameter slightly larger than 40 mm (for example, to cut it later to provide a better fit), then the number of cells in both horizontal directions must be even larger but always even (not odd). Although the CAD geometry for OPC samples can be easily built with any CAD tool, we provide *OpenSCAD* code for OPC samples in Table A.1 in Appendix A. This code automatically adheres to the above rules when the user sets only the cell size and sample diameter.

2.2. Four-Pore Cell geometry

The second periodic cell with open porosity is more complex than the previous one, because it was built randomly with four different pores using the algorithm proposed in [34]. The non-trivial construction of this Four-Pore Cell (FPC) is thoroughly discussed in Appendix B, and it ensures that for the assumed cell size $L_c = 5$ mm, the walls between neighbouring pores, as well as the edges of cylindrical channels connecting them, are thick enough to be correctly 3D printed using FFF devices. This and other key issues relevant to the FFF technology are studied, e.g. in [35].

The FPC contains pores of four different sizes, viz.: $0.53L_c$, $0.58L_c$, $0.60L_c$, and $0.68L_c$, which for the cell size $L_c = 5$ mm means the following values of pore diameters: 2.65, 2.90, 3.00, and 3.40 mm, respectively (cf. with 2.70 and 4.50 mm, i.e. the nominal pore diameters in OPC-3 and OPC-5, respectively). The nominal porosity for FPC (43.5%) is very similar to the porosity for OPC (43.7%). However, the

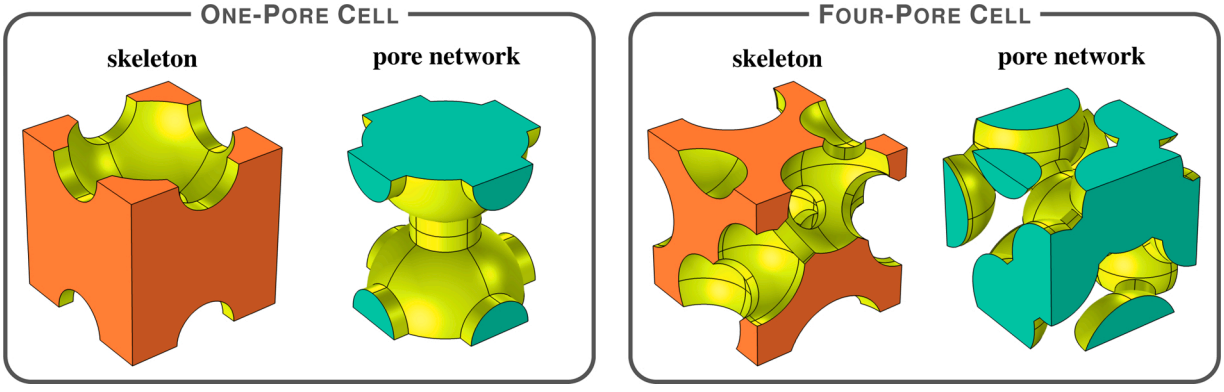

Fig. 3. Skeleton and the corresponding pore network for OPC (left) and FPC (right). (For interpretation of the references to color in this figure legend, the reader is referred to the web version of this article.)

pore and channel diameters in 3D printed samples, and consequently the actual open porosities are expected to be slightly smaller than the nominal values due to the 3D printing resolution, provided that there is no microporosity.

There are three orientations of FPC as shown in Fig. 2(a) (see also Fig. B.1 and the relevant explanations in Appendix B), namely: FPC-X, FPC-Y, and FPC-Z. The normalized data for the final FPC design are given in Table B.1 (in Appendix B) for the FPC-Z orientation. CAD models for FPC samples are generated for each orientation in a similar way as for OPC-5 samples (cf. Figs. 1(b) and 2(b)), but the cylinder height is 50 mm (not 60 mm), so for example, the CAD models for samples with a diameter of 29 mm shown in Fig. 2(c) were cut from three-dimensional arrays with $6 \times 6 \times 10$ (not 12) cells, see Fig. 2(b). We provide *OpenSCAD* code for FPC samples in Tables A.2 and A.3 in Appendix A. The cell size for FPC samples is set to 5 mm, so the user selects only the cell orientation and sets sample diameter.

2.3. OPC vs. FPC

The periodic geometries of OPC and FPC are compared in Fig. 3, where the solid part (i.e. 3D printed skeleton) and fluid part (i.e. pore network filled with air) of each periodic cell are depicted together. The interfaces between the solid and fluid domains are marked with a very bright (i.e. yellow) colour, while the periodic boundaries of the solid skeleton and fluid in the pores are marked with darker colours (i.e. orange for the solid and cyan for the fluid).

All porous samples produced for this study have rigid skeletons, because all input materials are sufficiently stiff and there are no very thin (membrane-like) walls nor thin ligaments in the proposed periodic cellular designs. Therefore, the only carrier for airborne acoustic waves penetrating porous samples is the air inside their open pore network (i.e. wave propagation in a solid skeleton is negligible), and the wave propagation and attenuation depend on the shape and size of the pore network.

Despite the fact that both periodic networks are made of spheres and cylinders (see Fig. 3), there are significant differences between them, in particular, from the point of view of visco-thermal transport, which directly affects the propagation and energy dissipation of airborne acoustic waves penetrating these networks. In periodic samples based on the OPC, see Fig. 3(left), spherical pores of the same size are linked with identical cylindrical channels, in particular the ones that are parallel to the direction of wave propagation, so that the permeability of this open porosity network is relatively high and the tortuosity is low. In the case of FPC, see Fig. 3(right), all four pores have different sizes and random positions, they are linked with cylindrical channels of various diameters, oblique (at various angles) to the wave propagation direction, so that the path of oscillatory flow caused by airborne acoustic waves should be very tortuous. For this reason, although the porosities of both periodic cells are almost identical, their tortuosities and permeabilities are very different, which entails significant differences in the propagation and absorption of airborne acoustic waves. To justify this, we briefly explain below how these non-acoustic properties are related to sound propagation in porous media [1,30].

The concept of tortuosity is used to characterize the structure of porous media, usually very geometrically complex. It is often treated as a geometric parameter and defined as the ratio of the average flow path length to the straight-line length across the porous medium [36], which means that it is greater than or equal to 1. The original definition of Carman [37] is the square of this value, and Bear [38], who even defines tortuosity as the inverse of the Carman's definition, argues that the square in the definition is necessary (see pp. 110–111 in Ref. [38]). On the other hand, tortuosity is also introduced in different ways as a parameter related to the hydraulic, electrical, or diffusive properties of the porous medium, which poses the fundamental question whether tortuosity is an intrinsic property of the porous medium or of a process within the medium. In practice, tortuosity is not consistently defined and various definitions are not unified in a coherent way [36]. Within the framework of the theory of sound propagation and absorption in fluid-saturated rigid porous media, the tortuosity appears in the formula for the effective fluid density, where it multiplies the actual density of the saturating fluid [1,30]. In that way, the presence of a rigid frame and associated inertial forces in the fluid virtually increase the effective density through the tortuosity parameter (greater than 1 for tortuous pore networks). This formula applies to the oscillatory flow of an inviscid fluid saturating the network of open pores, which in practice occurs in the high-frequency regime where the viscous boundary layers at the fluid-solid interface are extremely thin and viscous effects can be neglected. It can be shown that such an ideal, i.e. inviscid and incompressible flow formally coincides with the electrical problem of a porous dielectric material saturated with a conductive fluid [30]: the effective electrical conductivity of such a medium is directly proportional to the electrical conductivity of the saturating fluid, while inversely proportional to the tortuosity. This fact is used for the experimental determination of tortuosity [1], as well as for numerical calculations of tortuosity based on a representative geometry of the microstructure [30]. The concept of tortuosity is generalized for viscous oscillatory flows [39], which results in a complex-valued function of frequency, called dynamic viscous tortuosity, while the tortuosity parameter becomes the limit value for the frequency reaching infinity. The dynamic viscous tortuosity is inversely proportional to the so-called dynamic viscous permeability [39] (which is a generalization of the classic permeability parameter) and describes the frequency-dependent nature of the effective density of a rigid medium with open porosity saturated with viscous fluid that is the carrier of acoustic waves. Finally, thermal analogues of the dynamic viscous tortuosity and permeability are introduced [1,40,41], i.e. the dynamic thermal tortuosity and permeability, respectively, which allow determining the frequency-dependent effective compressibility of such a medium. The effective density and compressibility enable to determine the frequency-dependent and complex-valued effective speed of sound in a fluid-saturated rigid porous material, which takes into account the dispersion and wave attenuation phenomena associated with visco-thermal effects that occur on the micro-scale [1,30].

When comparing the pore networks of both cells (see Fig. 3), it is easy to see that due to the oblique channels, the geometric and viscous tortuosity should be much higher for FPC, which will strongly reduce the wave speed, and as a consequence should lower the frequencies of the so-called quarter-wavelength layer resonances [3]. At the same time the viscous permeability and characteristic length are lower, which should make the magnitude of peak absorption higher at the resonances. These expectations were confirmed by acoustic measurements (cf. OPC and FPC results in Section 5).

The main purpose of this study is to demonstrate that AM technologies can be used to produce and *independently reproduce* prototype samples to validate novel periodic designs of porous and meta-porous acoustic materials obtained from advanced microstructure-based modelling, which eventually should allow to optimize these designs. After optimization the resulting pore network may look very random. Therefore, for our round robin study we selected a relatively simple (regular) design and a more complex (irregular) random one. Both cellular designs should be easily reconstructed and may serve as benchmark examples (see also Appendix A).

3. Manufacturing of samples with periodic pore networks

3.1. 3D printers

Periodic porous samples with cellular designs proposed in Section 2 were fabricated in six AM technologies [6,7,9,11,42,43], which are listed in Table 1 along with the brand names of 15 different 3D printing devices used in this study, the corresponding materials as well as additional information such as sample manufacturers and labels used further

Table 1
3D printers used in the round robin study.

3D printing device	**Material**	**Laboratory (+ result labels & comments)**	
AM technology: Fused Filament Fabrication (**FFF**) a.k.a. Fused Deposition Modelling (**FDM**)			
Zortrax M200	ABS polymer filament	IPPT	(**FDM**-IPPT, dedicated filament *Z-ULTRAT*)
Flashforge Creator PRO	ABS polymer filament	IPPT	(**FFF**-IPPT, filament by *rigid.ink*)
Makerbot Replicator Z18	ABS polymer filament	UTC	(**FFF**-UTC)
Creality Ender 3	PLA polymer filament	TCD	(**FFF**-TCD)
Ultimaker 2	ABS polymer filament	TUe	(**FFF**-TUe*)
AM technology: Selective Laser Sintering (**SLS**)			
Sinterit Lisa	polyamide powder	IPPT	(**SLS**-IPPT, fine-grained powder)
3D Systems ProJet 160	polyamide powder	UTC	(**SLS-i**-UTC, cyanoacrylate-impregnated)
AM technology: Selective Laser Melting (**SLM**)			
EOS EOSINT M280	aluminium powder	IPPT	(**SLM**-IPPT, tape-wrapped samples)
3D Systems ProX	cobalt-chromium powder	TCD	(**SLM**-TCD, tape-wrapped samples)
Sisma MYSINT100	stainless steel powder	EMPA	(**SLM**-EMPA, tape-wrapped samples)
AM technology: Stereolithography (**SLA**)			
Formlabs Form 2	photopolymer resin	UTC	(**SLA**-UTC)
Formlabs Form 2	photopolymer resin	TCD	(**SLA**-TCD)
AM technology: Digital Light Processing (**DLP**)			
Autodesk Ember	photopolymer resin	MIT	(**DLP**-MIT*, **DLP**-MIT)
Kudo3D Titan 1	photopolymer resin	EMPA	(**DLP**-EMPA)
AM technology: LCD-based Stereolithography (**LCD** SLA)			
Zortrax Inkspire	photopolymer resin	IPPT	(**LCD**-IPPT)
Anycubic Photon	photopolymer resin	TCD	(**LCD**-TCD)

See Table 2 for full names of the laboratories

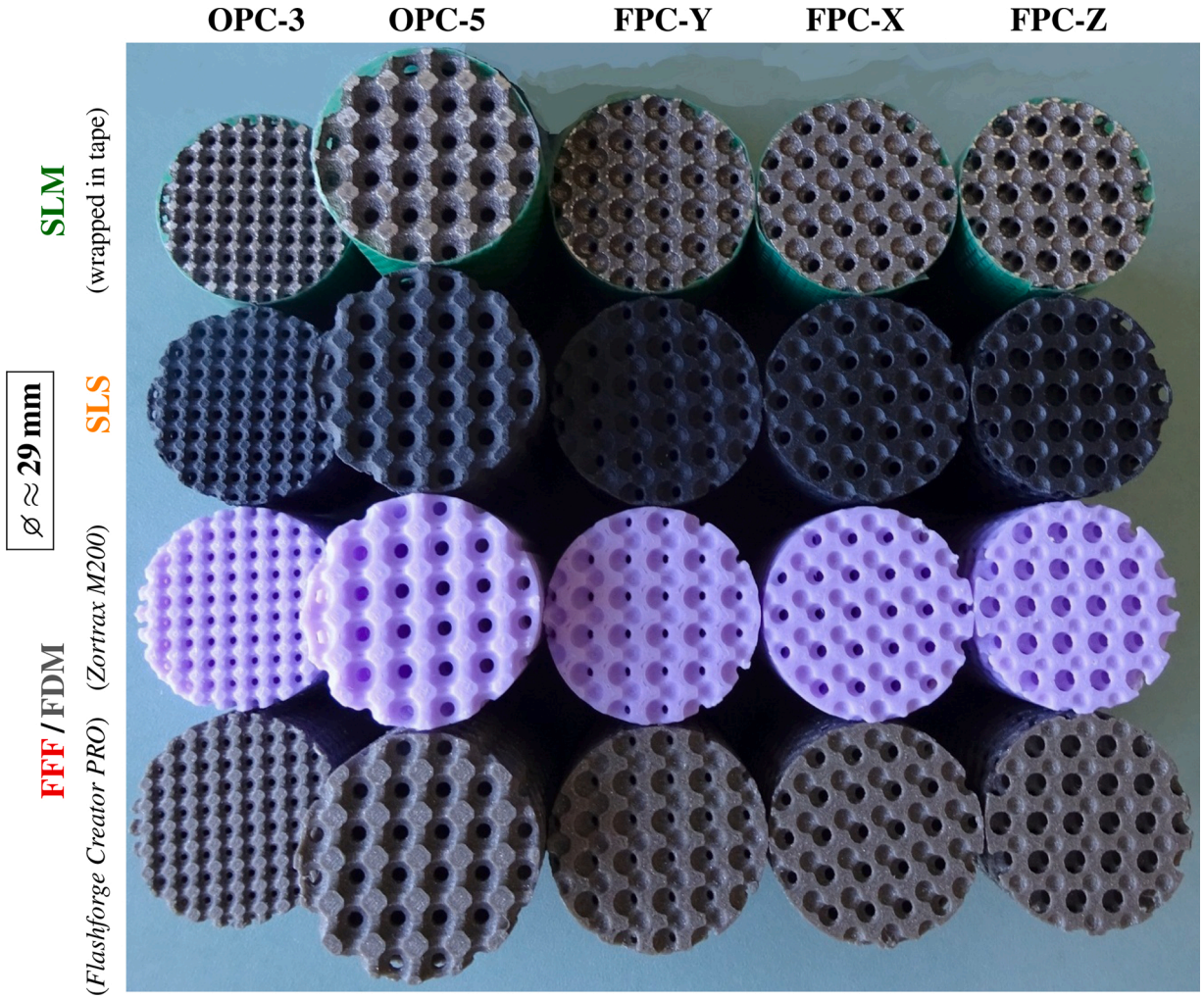

Fig. 4. Some of the OPC and FPC samples ($\phi \approx 29$ mm) manufactured by IPPT using various 3D printers. (For interpretation of the references to color in this figure legend, the reader is referred to the web version of this article.)

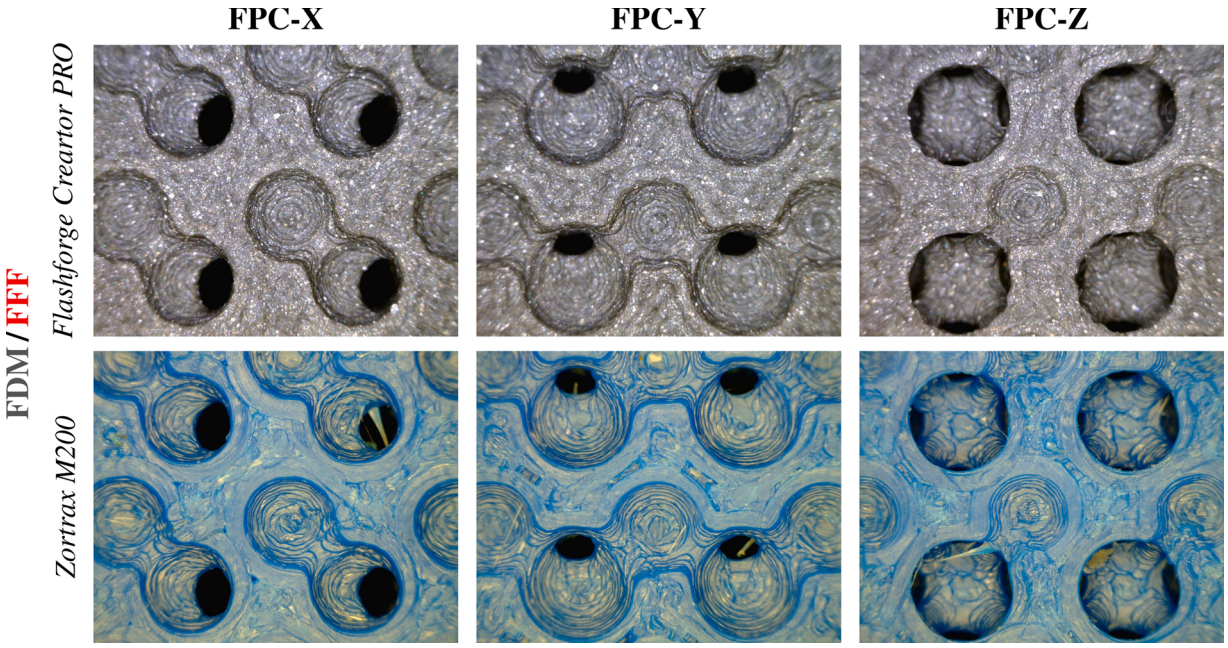

Fig. 5. Zoomed surfaces of FPC samples manufactured by IPPT using two different devices in the same technology.

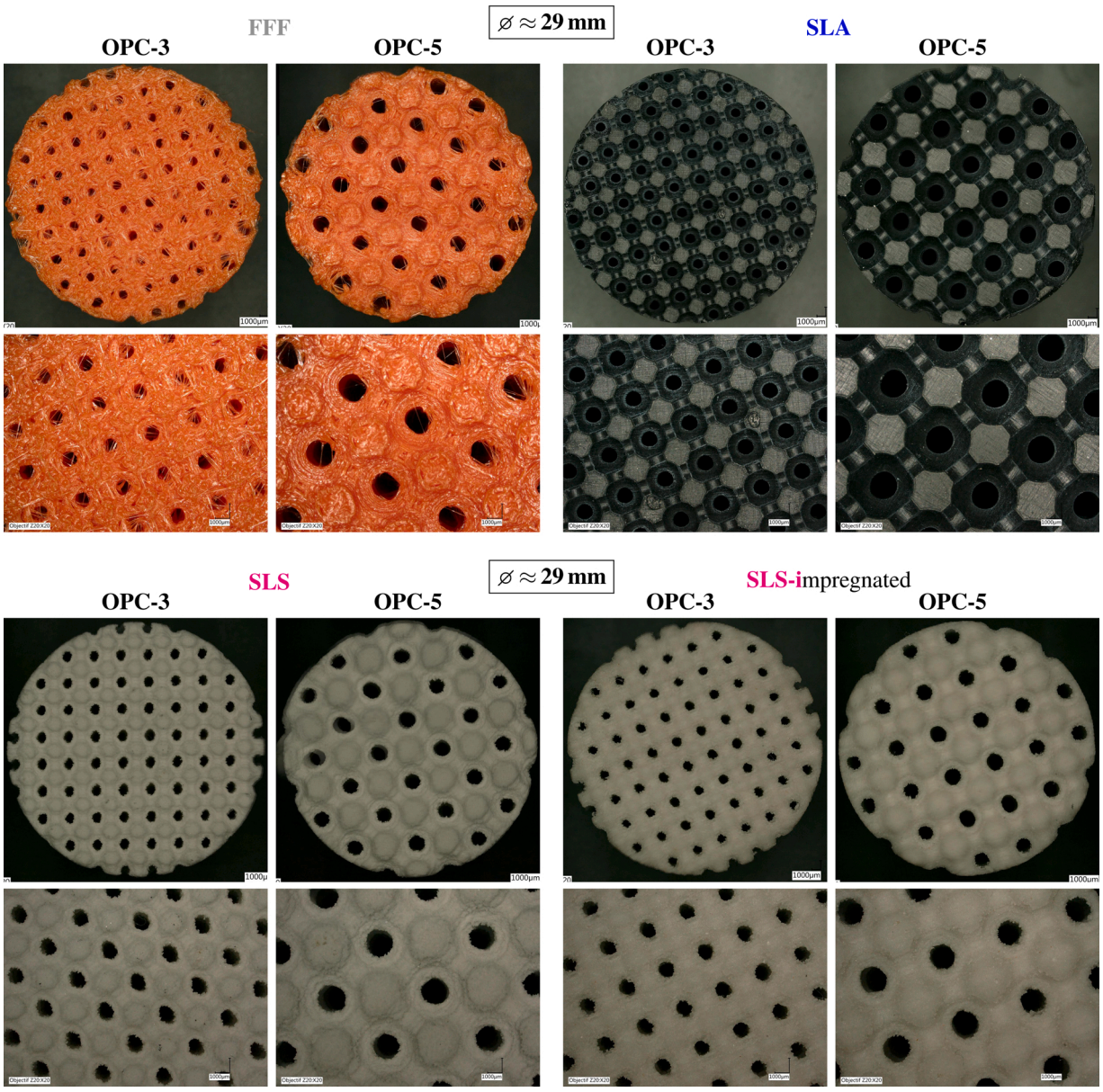

Fig. 6. OPC samples ($\phi \approx 29$ mm) manufactured by UTC using various technologies.

for marking measurement results.

The overall quality of some of the manufactured porous samples was assessed based on a series of measurements of crucial dimensions made with the aid of digital microscopes. It was observed that the designed micro-geometry was precisely reflected only for the case of the resin samples (SLA and LCD). Other technologies provided rough surfaces, indistinct edges, more or less degenerated pores (especially near the cylindrical surface of a sample), and were not able to capture important albeit intricate details. Furthermore, the spherical voids present in the cellular designs turned out to have smaller diameters than anticipated, and were distributed by unintended distances in structures other than resin-based. The reason for this is twofold: the highest printing resolution offered by SLA, LCD, and also DLP technologies (with the lower limit of 25 μm) and the usage of a liquid material. Nevertheless, resin samples must be carefully post-processed (cleaned and exposed to light for some time after fabrication to enhance their solidification) in order to avoid shrinkage over time. Because the LCD screen is composed of a number of pixels, the layers formed in the LCD technique consist of the so-called voxels, a spatial equivalent of pixels. This is why LCD prints are usually slightly more rough than the SLA ones, but still their quality is better when compared to the quality of samples fabricated in a low-resolution technique of FFF, or even in finer SLS and SLM techniques. It should also be noted that obtaining FFF samples with small details of decent quality usually requires some experience in the selection of materials and 3D printing parameters.

3.2. *Samples manufactured for impedance tubes with a diameter of 29 mm*

Periodic porous samples dedicated for 29 mm impedance tubes were manufactured by: (1) IPPT using FFF (*Zortrax M200* and *Flashforge Creator PRO*), SLS (*Sinterit Lisa*), SLM (*EOSINT 280*), and LCD (*Zortrax Inkspire*) technologies, (2) UTC using FFF (*Makerbot Replicator Z18*), SLS (*3D Systems ProJet 160*), and SLA (*Formlabs Form 2*) technologies, and (3) EMPA using *Kudo3D Titan 1* in DLP technology and *Sisma MYSINT100* in SLM technology (see Appendix C).

Complete sets of OPC and FPC samples were manufactured by IPPT in four completely different technologies. Fig. 4 shows some of these

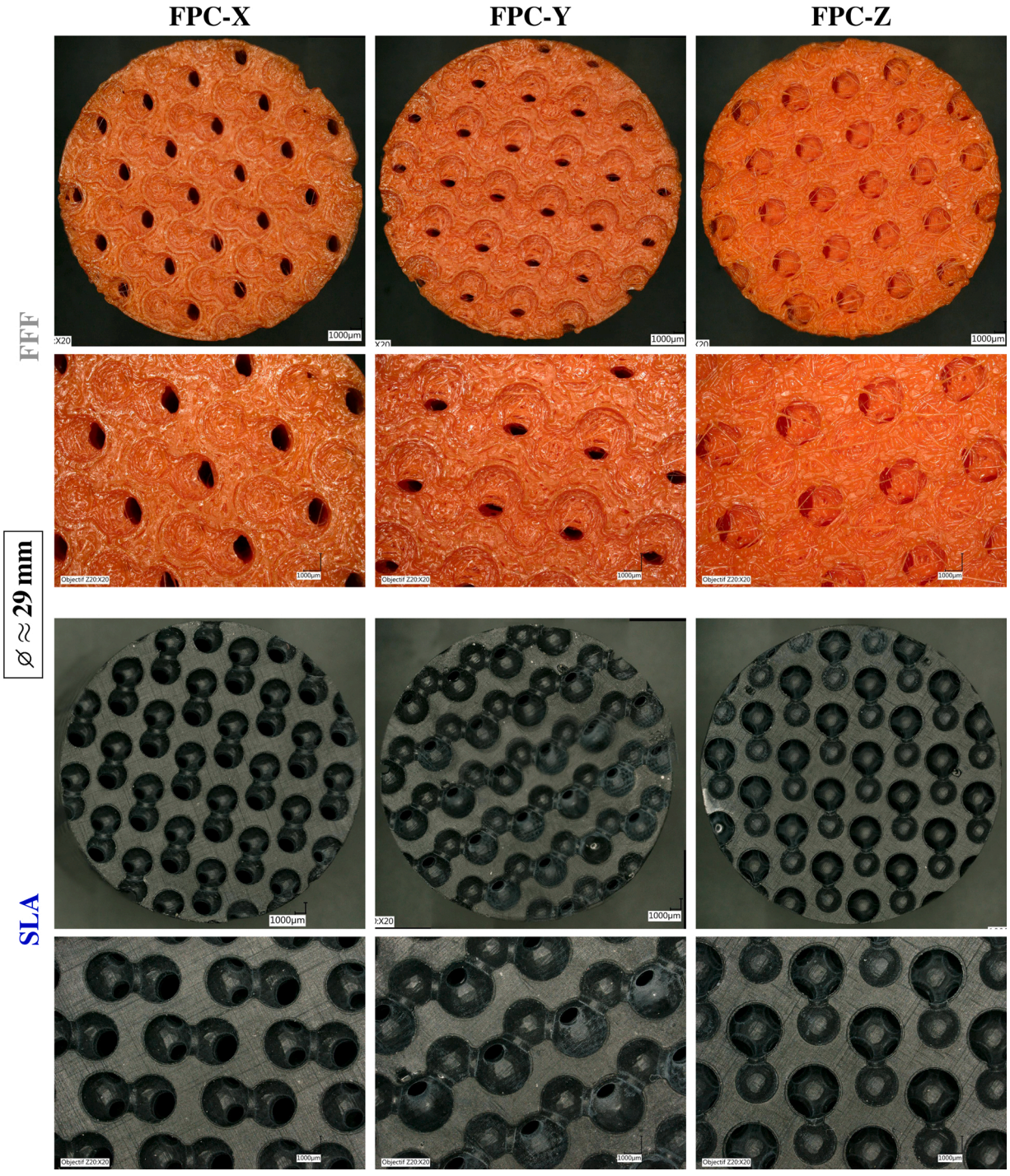

Fig. 7. FPC samples ($\phi \approx 29$ mm) manufactured by UTC using two different technologies.

samples (see also Fig. C.1 in Appendix C). It should be noted that two different FFF devices (*Zortrax M200* and *Flashforge Creator PRO*) were used to produce several sets of samples in this technology which allowed to observe that the quality and surface features of the samples obtained from the same AM device and material were virtually the same. On the other hand, one can easily notice differences between samples produced using different AM technologies and even different devices of the same technology FFF. This is well illustrated in Fig. 5 where surfaces for the FPC samples manufactured using *Flashforge Creator PRO* are compared with the ones from *Zortrax M200*. A relatively high quality of samples produced with *Flashforge Creator PRO* was obtained after many tests involving experimenting with 3D printing parameters and various high quality ABS (acrylonitrile butadiene styrene) materials from different producers (the final choice was *rigid.ink*), whereas a good quality of *Zortrax M200* samples was achieved using the dedicated high quality ABS material *Z*-ULTRAT and parameters set up for this material by the 3D printer manufacturer. The diameter of metal samples produced in SLM technology was deliberately chosen so that these samples loosely fit the 29 mm impedance tube and they must be wrapped in tape for a tight fit (see the green tape around these samples in Fig. 4). This had to be done (even knowing that the presence of the tape would affect the measurements) to avoid scratching the inside of the tube. The SLS samples were printed on *Sinterit Lisa* with a layer thickness equal 0.075 mm (the thinnest possible layer).

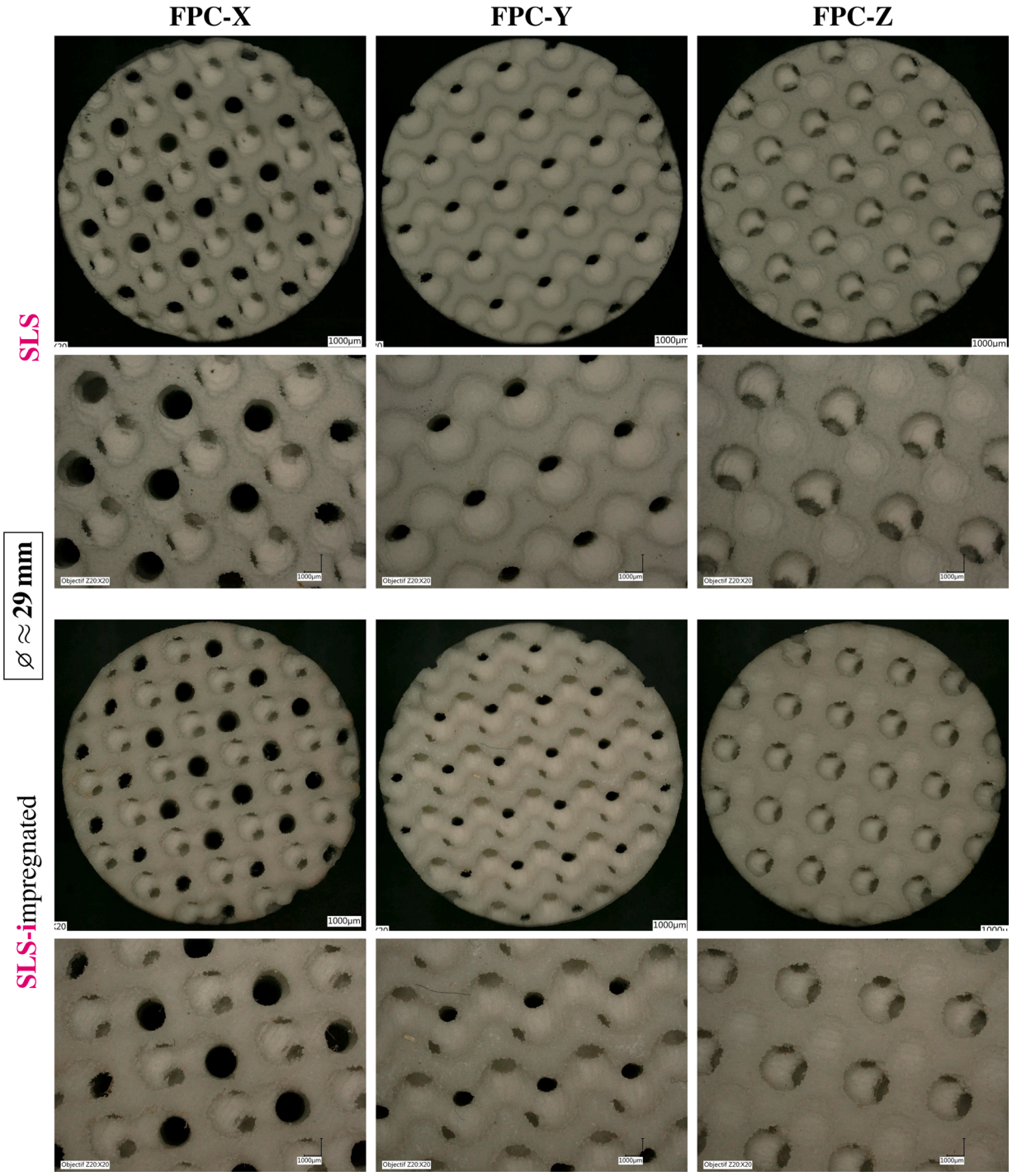

Fig. 8. FPC samples ($\phi \approx 29$ mm) manufactured by UTC from a polyamide powder.

Figs. 6–8 present the samples manufactured by UTC. This laboratory used three different AM technologies to produce complete sets of OPC (see Fig. 6) and FPC samples (see Figs. 7 and 8). However, in the case of SLS technology the samples were impregnated with cyanoacrylate to close the micro-pores that were present because of the relatively large grains of the polymer powder used in the sintering process, so that pictures of the SLS samples before and after impregnation are shown in Figs. 6 and 8 . Microscopic examinations of the samples (see enlarged photographs of their surfaces in Figs. 6–8) allowed to assess the relative quality of workmanship using different technologies. In the case of FFF samples the quality is generally poor (when compared to the FFF samples produced by IPPT): the channels and pores are distorted and the surface is rough with tiny polymer fibres which often run across the channels and pores. On the other hand, the shape and surface quality of SLA samples produced by UTC from photopolymer resin is excellent when compared with other technologies: the surfaces are very smooth and the shapes of circular channels and spherical pores are not distorted.

3.3. *Samples manufactured for impedance tubes with diameters of 40 and 30 mm*

Periodic porous samples for testing in 40 mm impedance tubes were manufactured by: (1) TCD using FFF (*Creality Ender 3*), SLM (*3D Systems ProX*), SLA (*Formlabs Form 2*), and DLP (*Anycubic Photon*) technologies,

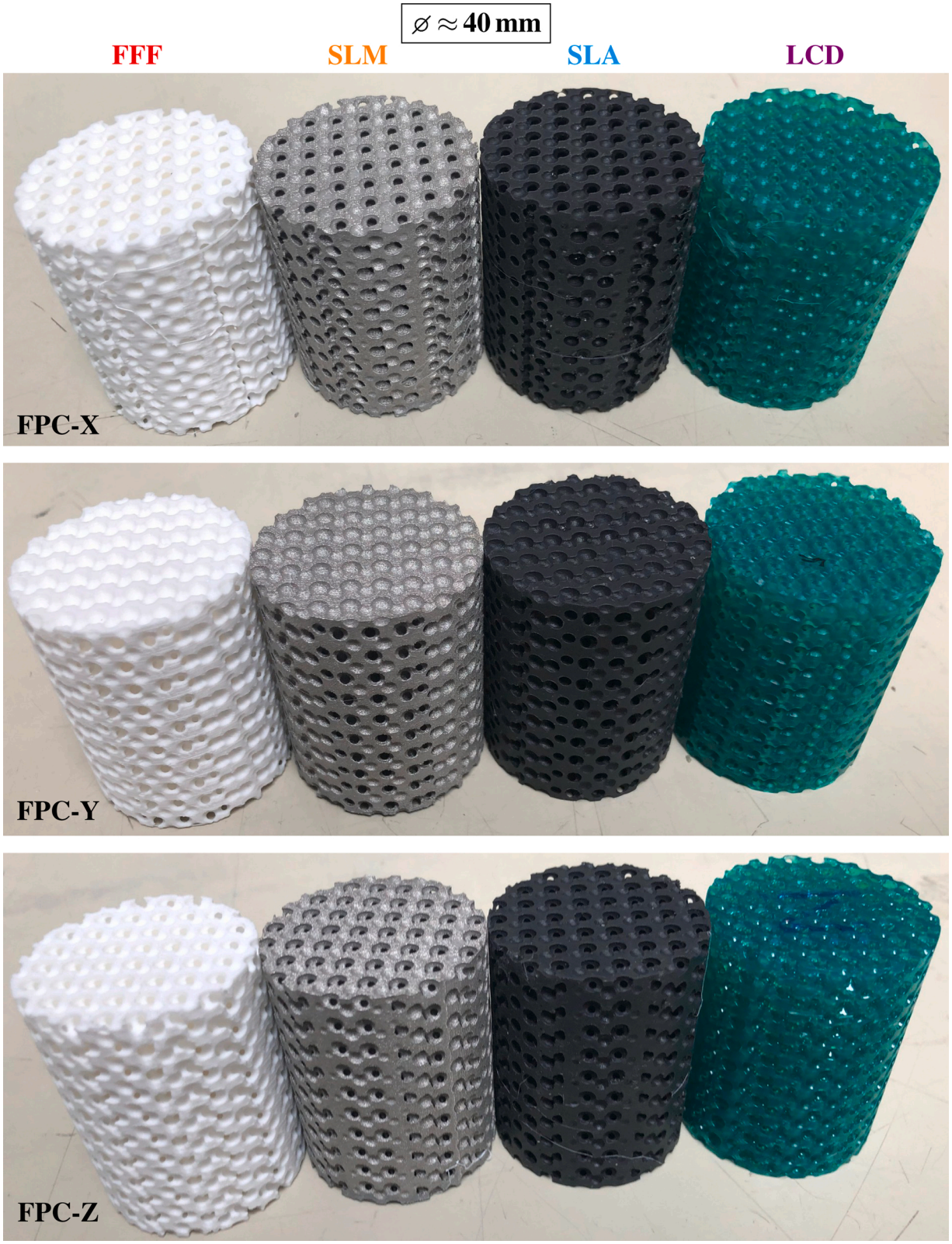

Fig. 9. FPC samples ($\phi \approx 40$ mm) manufactured by TCD using various technologies.

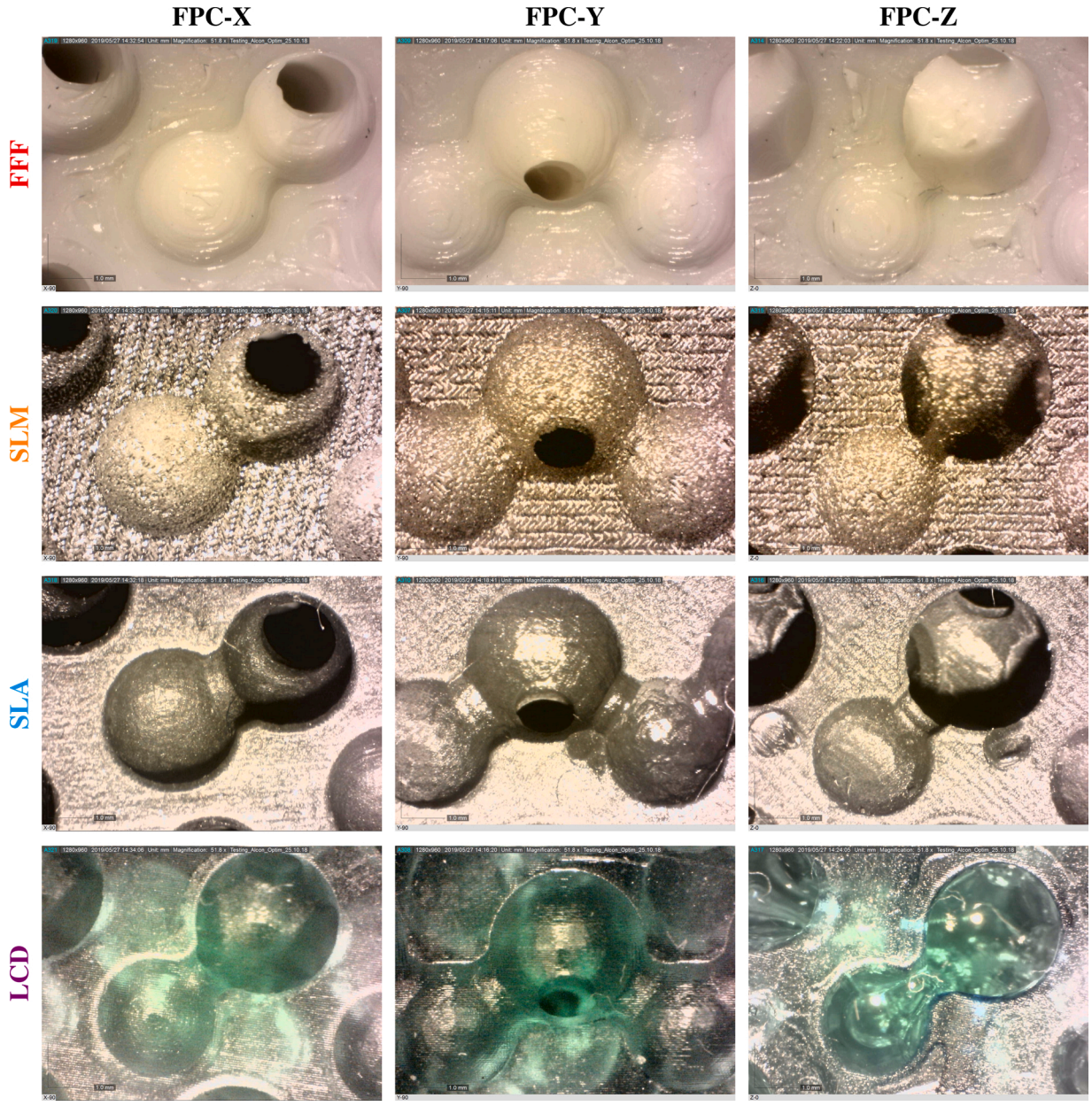

Fig. 10. Zoomed surfaces of FPC samples manufactured by TCD.

Table 2
Laboratories involved in the round robin manufacturing and testing of periodic porous samples, the corresponding impedance tube sizes, AM technologies and devices, types of materials, and manufactured samples (OPC = 2 samples: OPC-3 and OPC-5; FPC = 3 samples: FPC-X, FPC-Y, and FPC-Z).

Institution (laboratory)	**Tube size** ≈ sample ⌀	**FDM / FFF** polymer filaments	**SLS** polyamide powders	**SLM** metal powders	**SLA DLP LCD** photopolymer resins
IPPT	**⌀ 29 mm**	OPC [(1)], FPC [(1)] *Zortax M200 Flashforge Creator PRO*	OPC, FPC *Sinterit Lisa*	OPC, FPC *EOS EOSINT M280*	OPC *Zortrax Inkspire*
	⌀ 30 mm [(2)]	OPC, FPC *Zortax M200*	OPC, FPC *Sinterit Lisa*		
	⌀ 40 mm [(2)]	OPC, FPC *Zortax M200*	OPC, FPC *Sinterit Lisa*		
UTC	**⌀ 29 mm**	OPC, FPC *Makerbot Replicator Z18*	OPC [(3)], FPC [(3)] *3D Systems ProJet 160*		OPC, FPC *Formlabs Form 2*
EMPA	**⌀ 29 mm**			OPC, FPC *Sisma MYSINT100*	OPC, FPC *Kudo3D Titan 1*
MIT	**⌀ 30 mm**				OPC, FPC *Autodesk Ember*
TCD	**⌀ 40 mm**	FPC *Creality Ender 3*		FPC *3D Systems ProX*	FPC *Formlabs Form 2* FPC *Anycubic Photon*
TUe	**⌀ 40 mm**	OPC, FPC *Ultimaker 2*			

[(1)] A few complete sets of these samples were manufactured using two different FDM / FFF devices.
[(2)] IPPT only manufactured samples of this diameter (i.e. acoustic tests were carried out by another laboratory).
[(3)] These samples were acoustically tested and then impregnated with cyanoacrylate and tested again.

ECL	**⌀ 29 mm**	acoustical testing of samples from UTC and 29 mm samples from IPPT
LAUM	**⌀ 30 mm**	acoustical testing of samples from MIT and 30 mm samples from IPPT
KUL	**⌀ 40 mm**	acoustical testing of samples from TUe and 40 mm samples from IPPT

IPPT : Institute of Fundamental Technological Research of the Polish Academy of Sciences (Poland)
UTC : Université de Technologie de Compiègne (France)
EMPA : Swiss Federal Laboratories for Materials Science and Technology (Switzerland)
MIT : Massachusetts Institute of Technology (USA)
TCD : Trinity College Dublin (Ireland)
TUe : Eindhoven University of Technology (the Netherlands)
ECL : Ecole Centrale de Lyon (France)
LAUM : Laboratoire d'Acoustique de l'Université du Mans (France)
KUL : KU Leuven (Belgium)

(2) TUe using *Ultimaker 2* in FFF technology (see Appendix C), and (3) IPPT using *Zortrax M200* in FFF technology and *Sinterit Lisa* in SLS technology.

Fig. 9 presents the FPC samples produced by TCD from PLA polymer filament, metal powder, and photopolymer resins. The metal samples were manufactured from cobalt-chromium powder in SLM technology and wrapped with tape before being inserted into the impedance tube for acoustic testing. The pictures of top surfaces of these samples taken under a microscope are shown in Fig. 10. When comparing the resin samples it was observed that the quality of the ones manufactured in LCD technology was inferior than that of the samples made in SLA technology. This is mainly because some channels in LCD samples were clogged by the resin (in particular, in the case of the FPC-X sample) that was not completely removed.

Periodic porous samples for testing in 30 mm impedance tubes were manufactured by (1) MIT using *Autodesk Ember* in DLP technology (see Appendix C), and (2) IPPT using *Zortrax M200* in FFF technology and *Sinterit Lisa* in SLS technology.

4. Round robin investigations

Table 2 lists the nine laboratories involved in the round robin studies on sound-absorbing media with periodic open porosity produced using various Additive Manufacturing technologies. Six of these laboratories manufactured a different number of samples with diameters suitable for the impedance tubes used by them to measure acoustical properties of materials, viz.: 29 mm (IPPT, UTC, EMPA), 30 mm (MIT), and 40 mm (TCD, TUe). In addition, IPPT manufactured also sets of samples for tubes with diameters of 30 and 40 mm.

Six different AM technologies (FFF, SLS, SLM, SLA, DLP, LCD) were used to produce the samples from four kinds of input materials, namely: ABS and PLA polymer filaments, polymer powders, metal powders (aluminium, stainless steel, or cobalt-chrome), and photopolymer resins. The types of samples produced by each of the six laboratories are listed in Table 2 together with the appropriate AM technology and 3D printing device. Although the samples were acoustically tested by their manufacturers, in addition their acoustic properties were also measured in other laboratories, namely: the 29 mm samples produced by IPPT and UTC were independently tested by ECL, the 30 mm samples produced by MIT and IPPT were tested by LAUM, and finally, the 40 mm samples (delivered by TUe and IPPT) were tested by KUL. It should be noted that although IPPT produced samples for all considered impedance tube diameters (i.e. 29, 30, and 40 mm), it tested only those that fit in a 29 mm tube.

During the round robin investigations more than 90 samples were acoustically tested in impedance tubes, the majority of them in (at least) two different laboratories. In Appendix D we show a typical experimental configuration used in such tests along with the necessary explanations and other relevant information. The complete test for a single sample consisted in measuring the surface acoustic impedance and acoustic absorption for the sample in three or, in fact, six configurations. First, the sample was placed with its bottom face directly on the rigid termination of the impedance tube so that its upper face was impinged by acoustic plane waves at normal incidence. Then, an air gap of 20 mm was created between the sample and the rigid termination by moving the rigid plunger, and the measurement was repeated. A final measurement was taken for the case when the air gap was increased to 40 mm. This three-measurement procedure was repeated for the inverted sample so that its bottom face was exposed to incident plane acoustic waves. Inverted sample measurements generally confirmed the previous results very well, although especially in the case of FFF technology and metal samples, the bottom surface of a sample (which in one way or another is connected to the platform during the 3D printing process) usually slightly differs from the upper one. It was observed, however, that this effect was rather negligible since all discrepancies between the two measurements, i.e. in the standard and inverted position, were not significant and occurred at higher frequencies (above 5 kHz) where the other factors (i.e. material, manufacturing technology, etc.) are much more important and usually cause more discrepancies.

The round robin tests allowed to create a database of acoustical

Table 3
Result labels used in Figs. 11–19 and Figs. E.1–E.3, combined with the corresponding impedance tube diameters used for measurements, additive manufacturing devices and materials, and involved laboratories.

Result label	Tube size ≈ sample ⌀	*3D printing device* (& material)	Manufactured & tested by	Independently tested by
FDM-IPPT	⌀ **29 mm**	*Zortrax M200* (ABS polymer filament *Z-ULTRAT*)	IPPT	ECL
FFF-IPPT **FFF**-IPPT*		*Flashforge Creator PRO* (ABS polymer filament)	IPPT	ECL
SLS-IPPT **SLS**-IPPT*		*Sinterit Lisa* (polyamide powder)	IPPT	ECL
SLM-IPPT **SLM**-IPPT*		*EOS EOSINT M280* (aluminium powder)	IPPT	ECL
LCD-IPPT		*Zortrax Inkspire* (photopolymer resin)	IPPT	
FFF-UTC		*Makerbot Replicator Z18* (ABS polymer filament)	UTC	
SLS-i-UTC		*3D Systems ProJet 160* (polyamide powder, impregnated)	UTC	ECL
SLA-UTC **SLA**-UTC*		*Formlabs Form 2* (photopolymer resin)	UTC	ECL
DLP-EMPA		*Kudo3D Titan 1* (photopolymer resin)	EMPA	
SLM-EMPA		*Sisma MYSINT100* (stainless steel powder)	EMPA	
DLP-MIT **DLP**-MIT*	⌀ **30 mm**	*Autodesk Ember* (photopolymer resin)	MIT	LAUM
LCD-TCD	⌀ **40 mm**	*Anycubic Photon* (photopolymer resin)	TCD	
SLA-TCD		*Formlabs Form 2* (photopolymer resin)	TCD	
SLM-TCD		*3D Systems ProX* (cobalt-chromium powder)	TCD	
FFF-TCD		*Creality Ender 3* (PLA polymer filament)	TCD	
FFF-TUe*		*Ultimaker 2* (ABS polymer filament)	TUe	KUL

The asterisk symbol "*" means that the result was measured by a laboratory that did not produce the sample.

measurements obtained for samples manufactured in different AM technologies and measured by independent laboratories. The results were analysed and compared, in particular, for the samples with the same periodic cellular designs. Most representative results for most of the samples listed in Table 2 and described in Section 3 will be presented in Section 5, including even some of the results obtained for samples of evidently very poor quality to illustrate the resulting change in the nature of the sound absorption curves.

To facilitate quick identification of measurement results (presented in Section 5) and the corresponding samples the result labels used to denote the measurement curves are collected in Table 3 together with the corresponding tube (sample) diameter, AM device, material, manufacturer, etc. For example, the label "**SLA**-UTC" means that the result denoted in this way was measured in a 29 mm impedance tube for a resin sample manufactured by UTC in SLA technology using *Formlabs Form 2*, and the sample was tested by its manufacturer. A slightly modified label "**SLA**-UTC*" means that the result for this sample was measured by ECL, that is, a laboratory which did not produce the sample, but simply got it for independent testing from UTC. The sample micro-geometry (i.e. OPC-3, OPC-5, FPC-X, FPC-Y, or FPC-Z) is specified in each graph that compares the results obtained for samples with the same micro-geometry (and height). The only exception is the graphs in Fig. 16 where sound absorption for samples with different cell orientation is compared, and here the curve labels are complemented by a micro-geometry reference.

5. Measurement results

5.1. Sound absorption for OPC samples

Sound absorption measured for OPC-3 samples that were produced using six different AM technologies (viz.: FFF, SLS, SLM, LCD, SLA, and DLP) and various devices are compared in Fig. 11. Recall that the size of the cubic periodic cell in these samples is 3 mm, while their height is 36 mm. However, instead of being only backed by the rigid wall, the samples were also tested with air gaps set between the sample and the rigid plunger closing the impedance tube. Representative results for some of the samples backed with an air cavity of 40 mm are presented in Fig. 11(b).

Similarly, the results of acoustic absorption for OPC-5 samples (cell size: 5 mm, height: 60 mm) manufactured using various 3D printing devices are also compared for the mentioned configuration cases, i.e.: without air gap, or backed with an air gap of 40 mm (see Fig. 12). The discrepancies observed in Fig. 12(a) for the steel OPC-5 sample produced by EMPA are due to a slightly lower height of this specimen (i.e. closer to 58 mm than of 60 mm due to inaccurate cutting).

The results presented in Figs. 11 and 12 (see also Table 3 to decode the result labels) were measured in impedance tubes of two different sizes, namely, with a diameter of 29 and 30 mm. In the latter case, 30 mm samples were manufactured by MIT in DLP technology and tested by MIT as well as (independently) by LAUM. In the graphs, we present the absorption curves obtained by LAUM according to the ISO standard

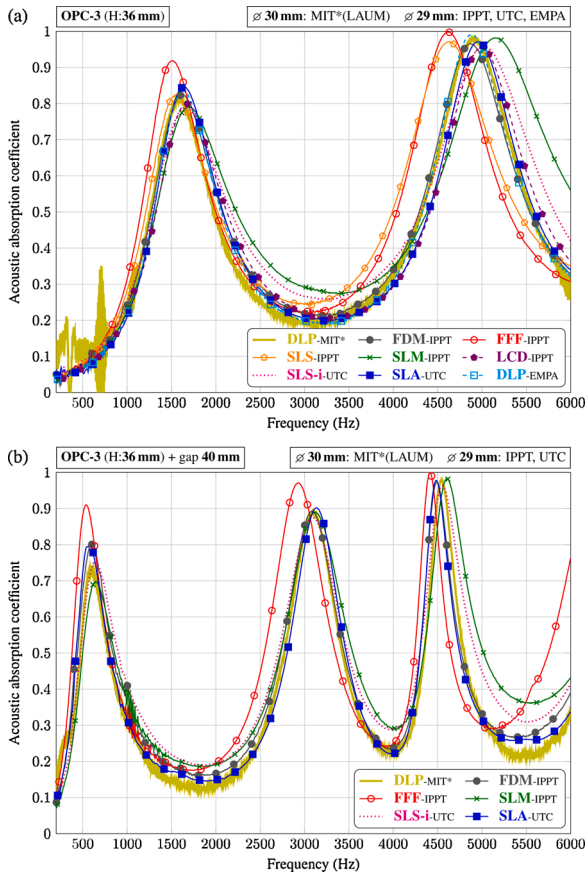

Fig. 11. Sound absorption measured for OPC-3 samples: (a) no air gap, (b) with an air gap of 40 mm.

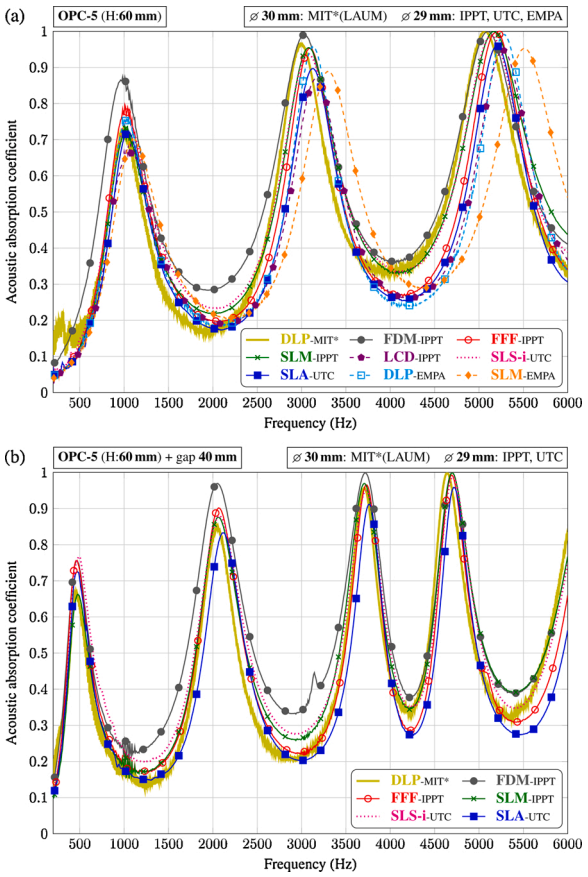

Fig. 12. Sound absorption measured for OPC-5 samples: (a) no air gap, (b) with an air gap of 40 mm.

[44]. They were virtually the same (though less fuzzy) as the curves provided by the manufacturer of samples who tested them according to the ASTM standard [45]. The absorption curves measured in 29 mm impedance tubes by IPPT and UTC (i.e. the manufacturers of samples) were very well confirmed by independent tests carried out by ECL. Although the samples were measured in different laboratories at slightly different conditions of pressure, temperature and humidity, discrepancies were very small indeed, and here we present only the curves obtained by the manufacturers.

A very good agreement is found between all curves measured for OPC-5 samples and between almost all curves obtained for OPC-3 samples. The frequencies of absorption peaks are consistent across all OPC-5 samples and the main discrepancies are in wide frequency ranges between the peaks where the resin samples (SLA, LCD, and also DLP) have the lowest absorption, which was rather expected since the surface of resin samples is smooth and without fibres or other important imperfections.

5.2. Sound absorption for FPC samples measured in tubes with a diameter of 29 mm

Figs. 13–15 compare sound absorption curves measured in tubes with a diameter of 29 mm for FPC-X, FPC-Y, and FPC-Z samples, respectively. The presented results (see Table 3 to decode the result labels) are obtained for samples (with a periodic cell size of 5 mm, and height of 50 mm) that were manufactured in four substantially different technologies (viz.: FFF, SLS, SLM, and SLA) using various devices available in three laboratories (IPPT, UTC, and EMPA). For almost all of these samples, in addition to the standard configuration with a rigid backing, the acoustic absorption was also measured in other configurations, in particular, when an air gap of 40 mm was added between the sample and the rigid end of the impedance tube. Most of these results are also shown in the graphs below. The following observations were made from a comparison of the corresponding absorption curves.

In general, a very good agreement is found between the absorption curves measured for the corresponding SLA samples (manufactured by UTC, and independently by EMPA), SLS samples (manufactured by IPPT), and high-quality FDM/FFF samples (by IPPT). Moreover, for most of these samples, rather unexpectedly, this consistency of measurement results applies throughout almost the whole frequency range considered (i.e. from 200 Hz up to nearly 6 kHz). Only for some of them, more significant discrepancies appear at higher frequencies above 4.5 kHz. This was, in fact, expected for FPC samples because their micro-geometry is more complex than in the case of OPC samples, and is therefore more prone to imperfections during the 3D printing process. It seems obvious that small inconsistent imperfections in micro-geometry should cause differences in measurements at higher frequencies.

A clear difference can be seen at medium and higher frequencies between the SLS samples manufactured by UTC and impregnated with cyanoacrylate, and the non-impregnated SLS samples manufactured by IPPT. Recall that SLS samples produced by UTC were sintered from a larger grain powder, which resulted in microporosity requiring

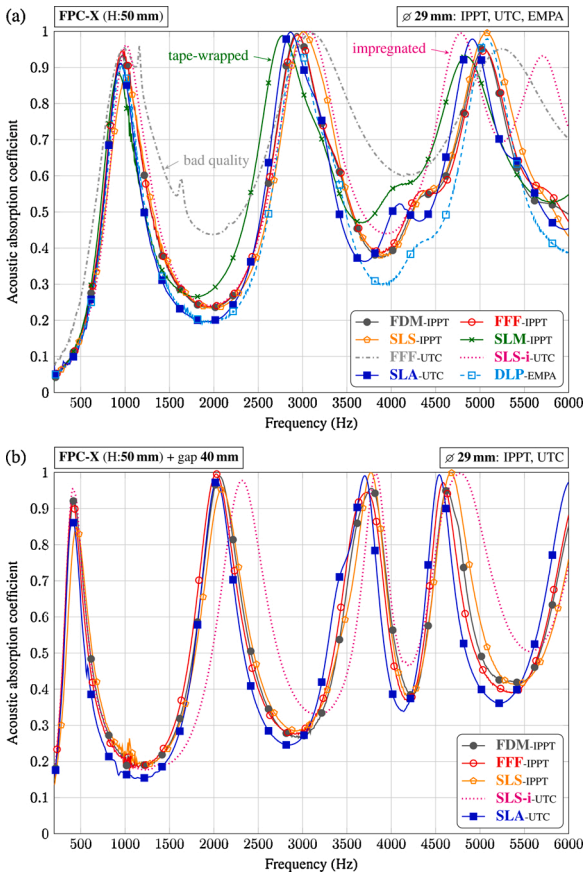

Fig. 13. Sound absorption measured for FPC-X samples: (a) no air gap, (b) with an air gap of 40 mm.

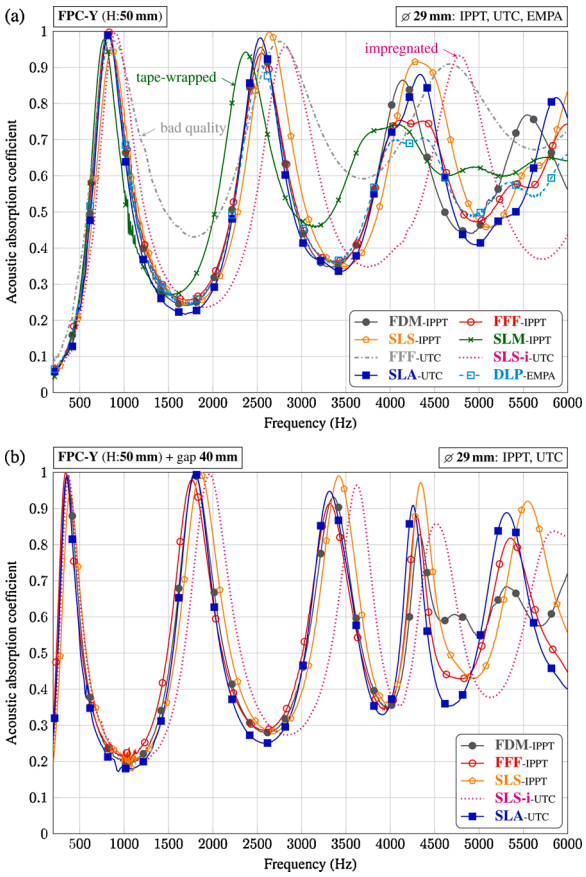

Fig. 14. Sound absorption measured for FPC-Y samples: (a) no air gap, (b) with an air gap of 40 mm.

impregnation [46,47]. For the impregnated samples, medium- and high-frequency absorption peaks are shifted to even higher frequencies. Although this discrepancy was not observed for OPC samples, it can be associated with impregnation in the case of FPC samples.

The absorption curves measured for FPC samples made of metal in SLM technology are only slightly different from most of the other curves: their second and third absorption peaks are shifted to slightly lower frequencies, and for FPC-Y and FPC-Z samples the curves become rather flat above 4 kHz. To some extent, these discrepancies may also be related to the fact that metal samples are wrapped with tape (to avoid scratching the tube).

In Figs. 13(a), 14(a) and 15(a), we also intentionally show the results obtained for poor quality FFF samples produced using *Makerbot Replicator Z18* from an ABS material suitable for printing shapes with not so small details. Even for these samples, the first absorption peaks (which appear below or near 1 kHz for FPC samples) are very well represented. On the other hand, the second and third absorption peaks are shifted to significantly higher frequencies, and the total absorption between the peaks is increased in the case of these FFF samples. All this is caused by imperfections (surface roughness, smaller pore and channel sizes, fibres inside the pores and across the channels) visible in enlarged photographs of these samples shown in Fig. 7.

Finally, in Fig. 16, we again present the results for FPC samples (as well as OPC-5 samples) manufactured by UTC in SLA technology and by IPPT in SLS technology, this time to directly compare sound absorption by samples with different FPC orientation, as well as sound absorption by OPC-5 samples. It can now be clearly seen that the curves obtained for the FPC-Y and FPC-Z samples are quite similar in nature compared to the FPC-X curve (in particular, their absorption peaks are shifted to relatively lower frequencies). Another observation is that the absorption peaks for OPC-5 samples are lower and shifted to higher frequencies compared to the absorption peaks for any FPC sample, despite the fact that the FPC samples are 10 mm shorter, while the porosity is almost identical for all samples. This expected result (see Section 2.3) is justified by the more tortuous and less permeable pore network in the FPC samples. Both graphs in Fig. 16 show, in fact, four pairs of absorption curves: two measurements for each of the three types of FPC sample (viz., orientation FPC-X, FPC-Y, and FPC-Z), as well as two measurements for each of the two OPC-5 samples. The first measurement in each pair is from the sample manufacturer (i.e. UTC or IPPT), while the second result was measured by ECL. It is easy to see that the differences between the measurements in each pair are insignificant and actually similar to the differences that usually occur when repeating acoustic tests for the same sample (in the same laboratory).

Surface acoustic impedance curves (real and imaginary parts) obtained from measurements for some FPC samples are presented and discussed in Appendix E.

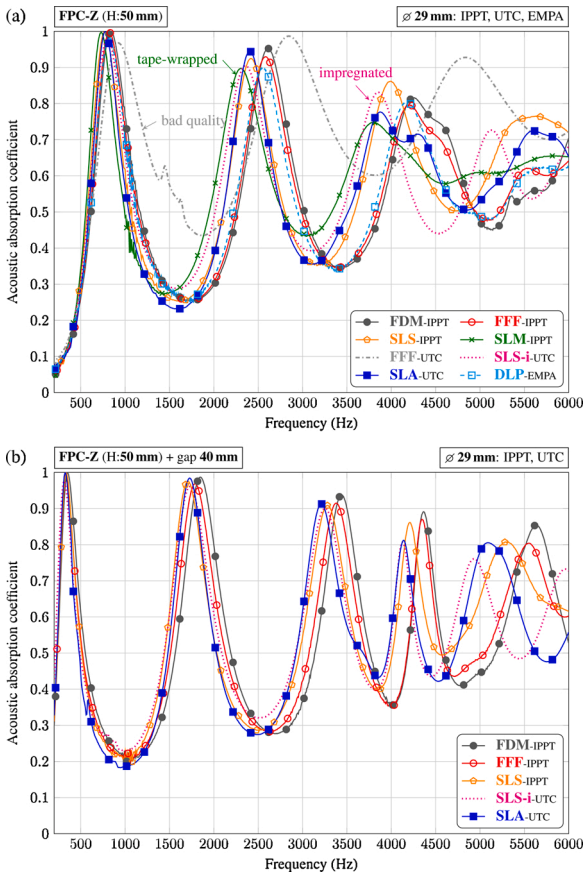

Fig. 15. Sound absorption measured for FPC-Z samples: (a) no air gap, (b) with an air gap of 40 mm.

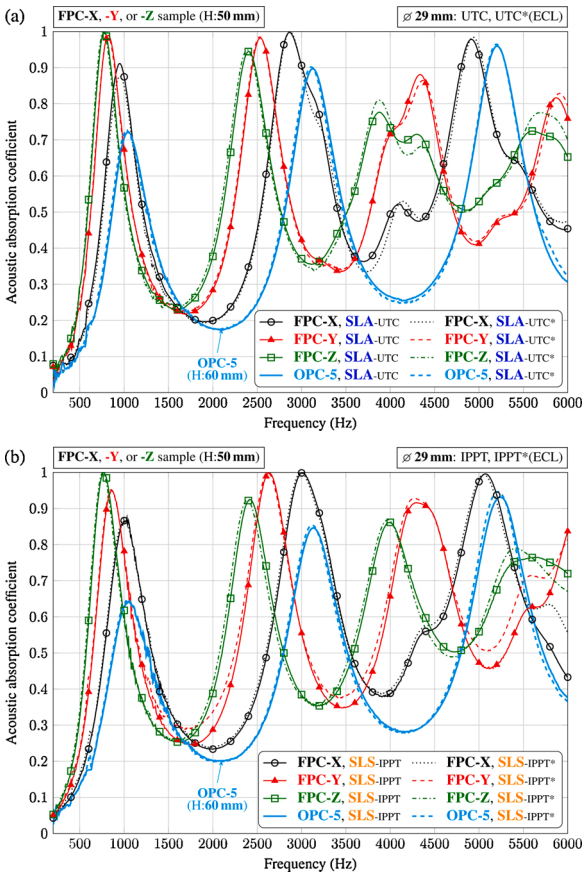

Fig. 16. Sound absorption measured for FPC and OPC-5 samples: (a) manufactured by UTC in SLA technology, (b) manufactured by IPPT in SLS technology. Two results are shown for each sample: one measured by the sample manufacturer and the other by ECL.

5.3. *Sound absorption for FPC samples measured in tubes with different diameters*

In Figs. 17–19 , acoustic absorption curves measured in 40 mm impedance tubes for FPC samples manufactured by TCD in FFF, SLM, SLA, and LCD technologies, and also for samples manufactured by TUe in FFF technology, are compared with each other and with the corresponding results measured in 30 mm tubes for FPC samples manufactured by MIT in DLP technology. In addition, several absorption curves measured in 29 mm impedance tubes for FPC samples manufactured by UTC in SLA technology and by IPPT in SLM technology, already shown in Section 5.2, are re-plotted as reference in the relevant graphs in Figs. 17–19, in the frequency range up to 4.5 kHz (valid for 40 mm impedance tubes). To decode the labels for specific results, see Table 3.

The general observation is that the discrepancy between the measurements of the corresponding 40 mm samples is greater than for most of the samples manufactured for tubes with a diameter of 29 mm. Also for 40 mm samples these discrepancies are already growing above 3.5 kHz. There are several reasons for this.

The quality of 40 mm FFF samples manufactured by TUe (and acoustically tested by KUL) is lower than that of the 29 mm FFF samples manufactured by IPPT using *Flashforge Creator PRO* or *Zortrax M200* (though it is better than the quality of samples 3D printed with *Makerbot Replicator Z18*). LCD samples are also of rather poor quality because some of the channels are clogged with resin that was not completely removed. Nevertheless, the agreement for the remaining resin samples (i.e. excluding the LCD ones) is rather good, as it is in the case of FFF

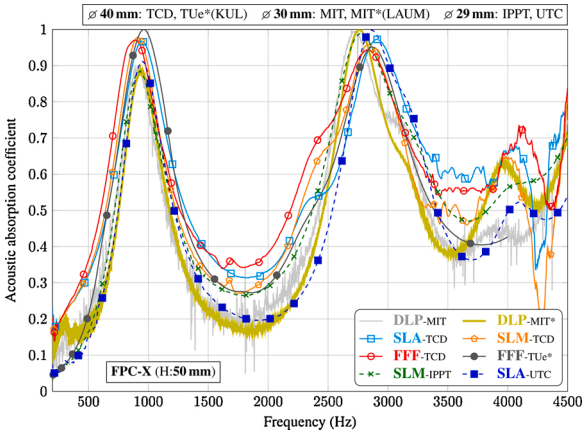

Fig. 17. Sound absorption measured in tubes with different diameters for FPC-X samples.

samples produced by TCD. It should also be noted that the absorption curves for 30 mm DLP samples are very similar to the sound absorption measured for 29 mm metal samples wrapped in tape.

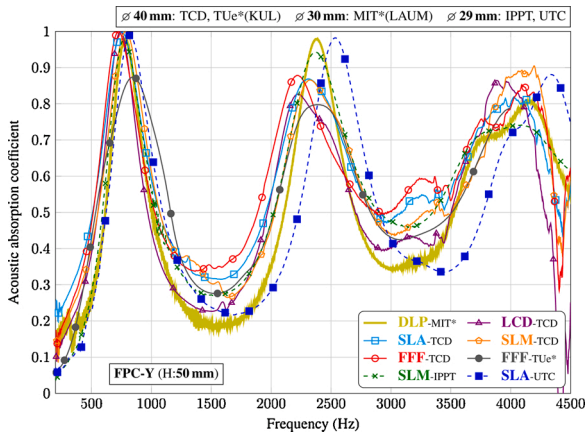

Fig. 18. Sound absorption measured in tubes with different diameters for FPC-Y samples.

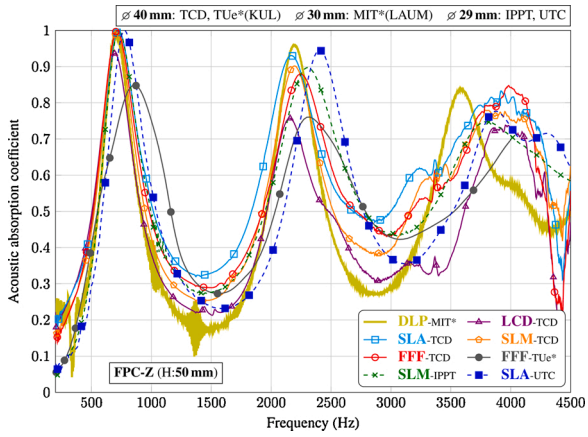

Fig. 19. Sound absorption measured in tubes with different diameters for FPC-Z samples.

6. Conclusions

Based on the examination of samples and comparison of measured sound absorption curves and surface acoustic impedance, we determined that there are three reasons for the discrepancy between the measurement results:

1. Overall manufacturing quality associated with AM technology and the material used for production. The main factor here is the correct (undistorted) reproduction of the designed micro-geometry related to the resolution of 3D printing (however, it should be remembered that the pore and channel diameters will always be slightly different than in the case of the CAD models used for 3D printing). Other factors are small imperfections (fibres, completely or partially clogged channels, microporosity, etc.) that appear during the production process, but also in a post-production treatment (due to difficulties in removing resin or powder, deformation during curing, problems with curing inner parts of resin porous samples), and sometimes even later (a delayed shrinkage effect).
2. Matching samples to the diameter of the impedance tube. This is a well-known reason for possible discrepancies [48,23]. When 3D printing samples for the impedance tube, one should proceed with caution as follows (to get a 'perfect' or exact fit, tight or only acceptable): (a) samples are 3D printed with slightly larger diameters than the diameter of the tube, and then cut to fit ('*perfect*', *exact*, or *tight* fit depending on the cutting method); (b) the sample diameter is determined by trial and error (for a specific AM device and material), so the samples can be 3D printed for a very tight fit (rather *tight* than *exact*, but can be sufficient if the cylindrical shape of the samples is not distorted); (c) samples are 3D printed with a slightly smaller diameter than the tube, and then wrapped with tape (acceptable, but should be avoided if possible).
3. The proposed periodic micro-geometries have relatively large features (i.e. large pores, wide channels), so the sample faces have large details around their circular edges, different for different sample diameters, because they depend on how the periodic cells are cut by the cylinder edge. This can affect the measurements.

Nevertheless, the overall consistency of the results measured for all good quality samples with the same periodic cellular designs proved to be good. We can also recommend SLA technology as the most suitable for manufacturing samples, because of the high accuracy of reproduction of designed periodic geometry, which is particularly suitable for prototyping and validating advanced acoustic modelling of porous and meta-porous materials with designed periodic geometry. On the other hand, the presented results show that for such relatively large cellular designs sufficient quality is achievable even when using FFF technology, provided that one has some experience (or luck) in matching the selection of parameters and materials for 3D printing.

The pronounced peaks in the absorption – clearly visible on the graphs – are associated with the so-called quarter (three-quarter, five-quarter, etc.) wavelength resonances related to the ratio between the wave length and the thickness of the porous layer [3]. For higher porosities, but with smaller pore sizes, absorption curves would become less "oscillating", i.e. peaks should not be so pronounced with much higher absorption between them. Obviously, the resonant frequencies (as associated with the frequency-dependent sound speed in a new porous medium) would also change.

High-tortuosity materials, such as FPC samples, are typically better acoustic treatments than less tortuous materials with the same porosity and similar sizes of the pore network (cf. the results for FPC and OPC-5 samples in Fig. 16). However, from the same reason it is more difficult to fabricate them, because of the complexity and tortuosity of their pore network. The difficulty is also largely related to the necessary post-processing treatment. For example, the FPC samples made from polyamide or metal powders had to be thoroughly cleaned with a high-pressure air compressor to remove powder residue from their open pore network. Otherwise, clogged channels would block the way for the oscillatory visco-thermal flow, and the acoustic waves would largely be reflected instead of being admitted, slowed down, and suppressed. It was even more difficult with samples fabricated from photopolymer resins (i.e. in the process of stereolithography or its variants). Such a sample must undergo an even more complicated post-processing treatment: first, the remaining liquid resin must be removed from the sample pores and channels, and then, the sample must be exposed to UV light to enhance its solidification. The winding geometry of the pore network (so desirable from the point of view of sound absorption) hinders these two stages of post-processing.

Small imperfections (such as roughness, small fibres inside voids, microporosity) tend to significantly increase sound absorption, which is usually desirable in applications (but not for model validation purposes). We believe that this can also be used to assess the 3D printing quality using acoustic measurements, like it was done, e.g. in [49]. It should be noted that, for example, the sound absorption between the peaks is very low, even at higher frequencies for samples with smooth surfaces without noticeable imperfections.

Authors' contribution

Tomasz G. Zieliński: conceptualization, methodology, software, investigation, resources, data curation, writing – original draft, writing – review & editing, visualization. Nicolas Dauchez and John Kennedy:

investigation, resources, visualization, writing – review & editing. Kamil C. Opiela, Piotr Pawłowski, Thomas Boutin, Daniel Trimble, Henry Rice, Bart Van Damme, Gwenael Hannema, Rafał Wróbel, Seok Kim, Shahrzad Ghaffari Mosanenzadeh, Nicholas X. Fang, Jieun Yang, Baltazar Briere de La Hosseraye, Maarten C.J. Hornikx: investigation, resources, visualization. Edouard Salze, Marie-Annick Galland, René Boonen, Augusto Carvalho de Sousa, Elke Deckers, Mathieu Gaborit and Jean-Philippe Groby: investigation, validation.

Conflict of interest

None declared.

Declaration of Competing Interest

The authors report no declarations of interest.

Acknowledgements

This work is based upon collaboration between the authors supported by European Cooperation in Science and Technology (COST) through the COST Action CA15125 – DENORMS: "*Designs for Noise Reducing Materials and Structures*". T.G. Zieliński and K.C. Opiela would also like to acknowledge the financial support from the National Science Centre (NCN), Poland, under Grant Agreement No. 2015/19/B/ST8/03979. The research of A. Carvalho de Sousa is funded by an Early Stage Researchergrant within the European Project ACOUTECT Marie Curie Initial Training Network (GA 721536). The research of E. Deckers is funded by a postdoctoral grant from the Research Foundation – Flanders (FWO).

Appendix A. Code listings for the CAD models of OPC and FPC samples

Table A.1 contains the code for the CAD models of OPC samples. The code for the CAD models of FPC samples is given in Tables A.2 and A.3 . These codes (see also Appendix F in the online verison) were provided to all laboratories that independently used them to generate STL files and G-codes for their 3D printers. They are in the *OpenSCAD* language [50,51] and we strongly recommend to use them with *FreeCAD* [52,53], because the *OpenSCAD* program may encounter problems rendering geometries composed of large arrays of periodic cells with many facets.

Table A.1
OpenSCAD code for periodic samples based on OPC.

```
// One-Pore-Cell periodic porous sample
// (2019) T.G.Zielinski

// Sizes of periodic elements
Lc = 5;        // cubic cell size [mm]
Dp = 0.9*Lc;  // pore diameter
Dw = 0.4*Lc;  // window diameter

// Sample (and cell array) dimensions
Ds = 29;                        // sample diameter [mm]
Nx = 2*ceil(0.5*ceil(Ds/Lc));  // Nx is even and Nx*Lc >= Ds
Ny = Nx;
Nz = 12;                        // numebr of cell layers
Hs = Nz*Lc;                     // sample height

// Flat-faces parameter (1 or 0)
FFP = 0;

// Auxiliary shifts
Xsh = -0.5*(Nx+1)*Lc;
Ysh = -0.5*(Ny+1)*Lc;
Zsh = -0.5*Lc*FFP;

// Periodic cell
module PeriodicCell(Nfacets=16) {
    difference() {
        cube(size=Lc, center=true);
        sphere(d=Dp, $fn=Nfacets);
        cylinder(h=Lc, d=Dw,  $fn=Nfacets, center=true);
        rotate(a=90, v=[1,0,0])
            cylinder(h=Lc, d=Dw, $fn=Nfacets, center=true);
        rotate(a=90, v=[0,1,0])
            cylinder(h=Lc, d=Dw, $fn=Nfacets, center=true);
    }
}

// PeriodicCell(32);  // Use 0 facets for FreeCAD, 32 for OpenSCAD.
// To generate only a single periodic cell uncomment the line above
// and delete (or comment) all the lines below.

// Cylindrical sample
intersection() {
    cylinder(d=Ds, h=Hs, $fn=128);
    for (nx=[1:1:Nx], ny=[1:1:Ny], nz=[FFP:1:Nz]) {
        translate([nx*Lc+Xsh, ny*Lc+Ysh, nz*Lc+Zsh])
            PeriodicCell(0);  // Use 0 facets for FreeCAD.
    }
}
```

Table A.2
OpenSCAD code for periodic samples based on FPC.

```
// Four-Pore-Cell periodic porous sample
// (2019) T.G.Zielinski

// PERIODIC POROUS CELL
// Cell size and orientation (rotation)
Lc = 5;         // cubic cell size [mm]
XYorZ = "Z";   // orientation (set "X", "Y", or "Z")
// Rotation axis and angle
RotAxis  = (XYorZ=="X") ? [0,1,0] : (XYorZ=="Y") ? [1,0,0] : [0,0,1];
RotAngle = (XYorZ=="Z") ? 0 : 90;

// Pore size scaling factor
PSSF = 0.9;

// Normalised data for pores (initial diameters + positions)
// Pore 1
d1 = 0.59;                                  // (initial diameter)
x1 = 0.00;    y1 = 0.00;    z1 = 0.00;      // (coordinates)
p1 = [x1,y1,z1];                            // (position)

// Pore 2
d2 = 0.64;                                  // (initial diameter)
x2 = -0.47;   y2 = -0.44;   z2 = 0.04;      // (coordinates)
p2 = [x2,y2,z2];                            // (position)

// Pore 3
d3 = 0.67;                                  // (initial diameter)
x3 = 0.45;    y3 = -0.05;   z3 = -0.35;     // (coordinates)
p3 = [x3,y3,z3];                            // (position)

// Pore 4
d4 = 0.76;                                  // (initial diameter)
x4 = 0.04;    y4 = -0.51;   z4 = 0.37;      // (coordinates)
p4 = [x4,y4,z4];                            // (position)

pos = [
    [p1, [0, 0, 0]],
    [p2, [0, 0, 0], [ 1, 0, 0], [0, 1, 0], [ 1, 1, 0]],
    [p3, [0, 0, 0], [-1, 0, 0], [0, 0, 1], [-1, 0, 1]],
    [p4, [0, 0, 0], [ 0, 1, 0], [0, 0,-1], [ 0, 1,-1]],
];

Diameters = [d1, d2,d2,d2,d2, d3,d3,d3,d3, d4,d4,d4,d4];
Positions = Fun1(len(pos),pos);

function Fun1(n,X) =
    ( n==0 ? [] : concat(Fun1(n-1,X), Fun2(len(X[n-1])-1,X[n-1])) );

function Fun2(n,X) =
    ( n==0 ? [] : concat(Fun2(n-1,X), [X[0]+X[n]]) );

// Window diameter between two pores (NaN for non-overlapping pores)
function WindowDiameter(P1, D1, P2, D2) =
    let(
    R1R1 = 0.25*D1*D1,  R2R2 = 0.25*D2*D2,
    dd = pow(norm(P1-P2),2),
    xi = ( dd + R1R1 - R2R2 )/(2*dd)
    )
    2*sqrt( R1R1 - xi*xi*dd );

// To be continued in the next Listing ...
```

Table A.3
Continuation of the code from Table A.2.

```
// ... continuation of the previous Listing.

// Cylinder between two points
module CylinderBetweenPoints(P1, P2, D, Nfacets=16) {
    PP = P2-P1;  x = PP[0];  y = PP[1];  z = PP[2];
    height = norm(PP);       // cylinder height
    beta = acos(z/height);   // inclination angle
    gamma = atan2(y,x);      // azimuthal angle
    translate(P1){
        rotate([0, beta, gamma])
            cylinder(h=height, d=D, $fn=Nfacets);
    }
}

// Periodic cell (skeleton)
module PeriodicCell(Nfacets=16) {
    rotate(a=RotAngle, v=RotAxis)
    difference() {
        cube(size=Lc, center=true);
        union() {
            N = len(Diameters)-1;
            for(m = [0:1:N]) {
                Pm = Positions[m];
                Dm = Diameters[m];
                dm = round(PSSF*100*Dm)/100;
                translate(Pm*Lc) sphere(d=dm*Lc, $fn=Nfacets);
                for(n = [(m+1):1:N]) {
                    Pn = Positions[n];
                    Dn = Diameters[n];
                    Dw = WindowDiameter(Pm, Dm, Pn, Dn);
                    if(Dw>0) {
                        dw = round(100*Dw)/100;
                        CylinderBetweenPoints(Pm*Lc, Pn*Lc, dw*Lc, Nfacets);
                    }
                }
            }
        }
    }
}

// PeriodicCell(32);  // Use 0 facets for FreeCAD, 32 for OpenSCAD.
// To generate only a single periodic cell uncomment the line above
// and delete (or comment) all the lines below.

// CYLINDRICAL PERIODIC POROUS SAMPLE
// Sample (and cell array) dimensions
Ds = 29;                        // sample diameter [mm]
Nx = 2*ceil(0.5*ceil(Ds/Lc));  // Nx is even and Nx*Lc >= Ds
Ny = Nx;
Nz = 10;                        // numebr of cell layers
Hs = Nz*Lc;                     // sample height

// Cylindrical sample
nNx = [-0.5*(Nx-1) : 1 : 0.5*(Nx-1)];
nNy = [-0.5*(Ny-1) : 1 : 0.5*(Ny-1)];
nNz = [0.5 : 1 : (Nz-0.5)];
intersection() {
    cylinder(d=Ds, h=Hs, $fn=128);
    union() {
        for (nx=nNx, ny=nNy, nz=nNz)
            translate([Lc*nx, Lc*ny, Lc*nz])
                PeriodicCell(0);  // Use 0 facets for FreeCAD.
    }
}
```

Appendix B. Construction of the Four-Pore Cell

A periodic arrangement of four spherical pores of different sizes in a cubic cell was randomly generated using the algorithm proposed in [34]. The central point of the cubic cell was moved to the centre of the smallest pore, and the whole system was scaled (normalized), so that the size (i.e. edge) of the cubic cell is 1. Then, the normalized positions (centres) and pore diameters were rounded to two decimal places. The obtained normalized values of pore diameters, i.e. 0.59, 0.64, 0.67, and 0.76, respectively, will be reduced by 10% for the reasons explained below. Because the pore diameter is smaller than the size of a cubic cell, only one instance of central pore appears in the cubic cell. On the other hand, for each of the other three pores, four periodically shifted pore instances are partly in the same cubic cell, which means that together there are 13 instances of 4 different pores in such a Fore-Pore Cell (FPC). This initial FPC design is shown in the top frame in Fig. B.1 for three different orientations of the periodic cell. The bottom row in this frame shows the results of analyses carried out by the *Z-SUITE* slicing software (dedicated for *Zortrax* 3D printers) for the periodic cell scaled to the size of 5 mm. These analyses show that the wide fragments of the edges around the windows connecting the pores are too thin to be properly 3D printed using *Zortrax M200* 3D printer (or other FFF devices with a standard nozzle size of 0.4 mm), and undesigned windows (holes) will also be created, because some parts of the wall between the pores are too thin. Therefore, the diameters of all the pores were reduced by 10% and rounded again to two decimal places (see the middle frame in Fig. B.1), and then cylindrical channels were set between each pair of pores that were originally connected by windows. To accurately re-create these connections, the normalized diameters of the cylindrical channels were set to the values found for the windows in the initial design (rounded to two significant digits). In this way, the edges of the windows are now thick enough so that they can be correctly manufactured using FFF devices (see the final design in the bottom frame in Fig. B.1).

All the necessary data for the final FPC design are given in Table B.1 in the form of normalized values that have to be scaled, i.e. multiplied by $L_c = 5$ mm, which is the size (length of the edge) of the cubic cell. These data are for the cell orientation designated FPC-Z, because the axis of the porous cylinder of the corresponding FPC-Z sample is along the *Z*-axis. Two other orientations are: FPC-X when the axis of the porous cylinder of the respective sample is along the *X*-axis, and FPC-Y when it is along the *Y*-axis. The porous cylinders are upright, so in practice the FPC cell is rotated, namely: the FPC-X cell is obtained by rotating FPC-Z cell by 90° around the *Y*-axis, while the FPC-Y one by rotating the FPC-Z cell by 90° around the *X*-axis.

Table B.1
Data for the FPC geometry with the cubic cell centred on `[0,0,0]` and edge length `1`. To get the actual dimensions, the values in the tables below should be multiplied by the cell size (e.g. 5 mm).

Diameters of pores and positions for relevant pore instances (dimensionless values, normalised by cell size)

No.	Pore instance	Pore diameter	Coordinates of the pore centre $[x, y, z]$		
1	P1-1	0.53	0.00	0.00	0.00
2	P2-1	0.58	−0.47	−0.44	0.04
3	P2-2	0.58	0.53	−0.44	0.04
4	P2-3	0.58	−0.47	0.56	0.04
5	P2-4	0.58	0.53	0.56	0.04
6	P3-1	0.60	0.45	−0.05	−0.35
7	P3-2	0.60	−0.55	−0.05	−0.35
8	P3-3	0.60	0.45	−0.05	0.65
9	P3-4	0.60	−0.55	−0.05	0.65
10	P4-1	0.68	0.04	−0.51	0.37
11	P4-2	0.68	0.04	0.49	0.37
12	P4-3	0.68	0.04	−0.51	−0.63
13	P4-4	0.68	0.04	0.49	−0.63

Diameters of channels between pore instances (dimensionless values, normalised by cell size)

Pore instance	Pore instance	Channel diameter
1 (P1-1)	6 (P3-1)	0.26
1 (P1-1)	10 (P4-1)	0.24
1 (P1-1)	11 (P4-2)	0.27
2 (P2-1)	7 (P3-2)	0.34
2 (P2-1)	10 (P4-1)	0.34
3 (P2-2)	6 (P3-1)	0.34
3 (P2-2)	10 (P4-1)	0.37
4 (P2-3)	11 (P4-2)	0.34
5 (P2-4)	11 (P4-2)	0.37
6 (P3-1)	12 (P4-3)	0.23
8 (P3-3)	10 (P4-1)	0.23

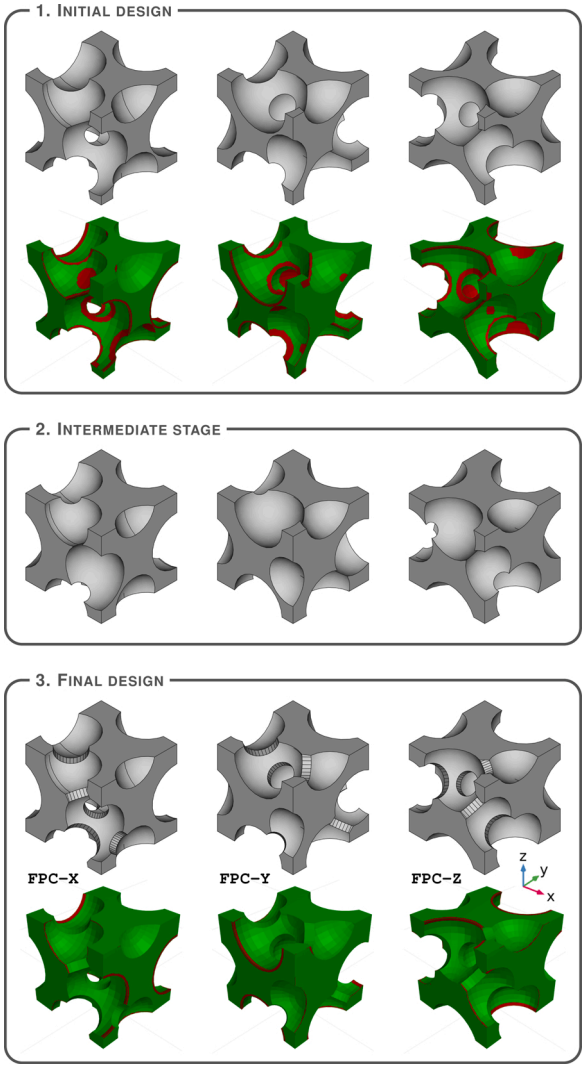

Fig. B.1. Four-Pore Cell (FPC) geometry: a re-design procedure and three orientations.

Appendix C. More 3D printed samples

Fig. C.1 shows perspective views of some samples with a diameter of 29 mm, fabricated by IPPT from ABS thermoplastic polymer, polyamide powder, aluminium powder (wrapped in protective tape), and photopolymer resins (in LCD SLA technology).

Fig. C.2 presents complete sets of high-quality OPC and FPC samples ($\phi \approx 29$ mm) produced by EMPA from photopolymer resin using DLP technology, as well as metal samples from stainless steel powder (SLM technology). For acoustic testing, the metal samples were wrapped with tape to securely fit them into the impedance tube.

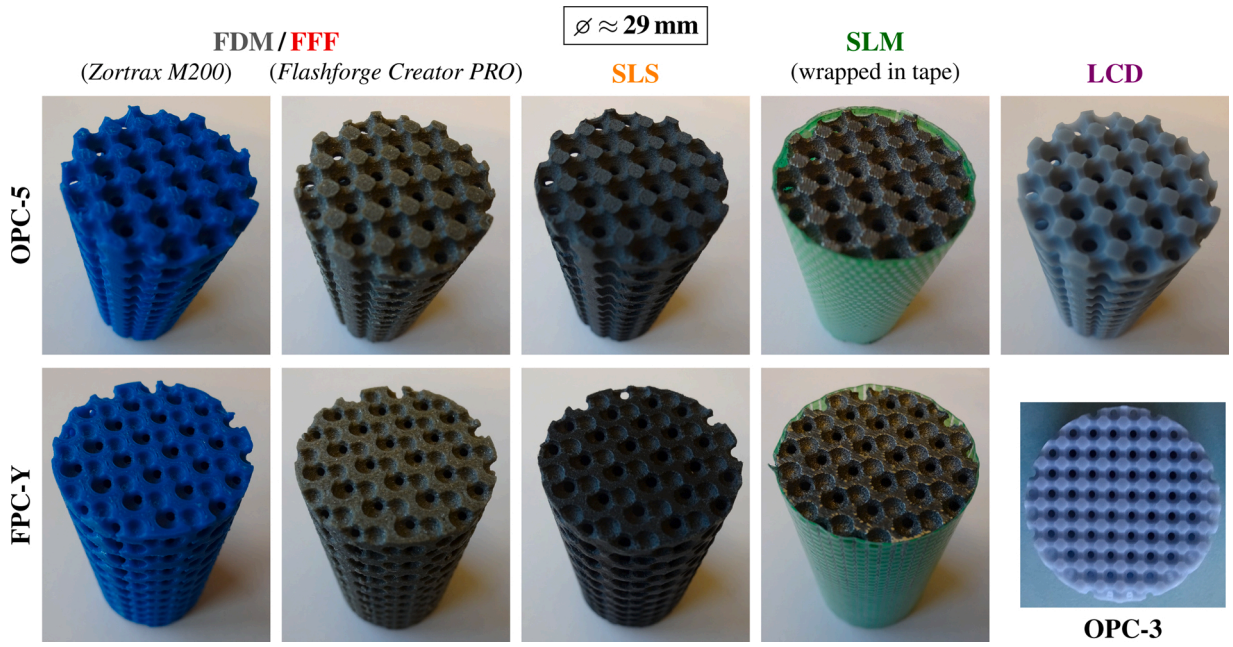

Fig. C.1. Some of the OPC and FPC samples ($\phi \approx 29$ mm) manufactured by IPPT using various 3D printers.

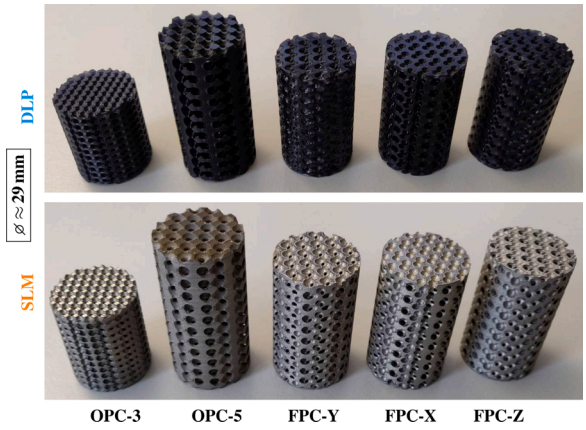

Fig. C.2. OPC and FPC samples ($\phi \approx 29$ mm) manufactured by EMPA from a photopolymer resin and stainless steel powder.

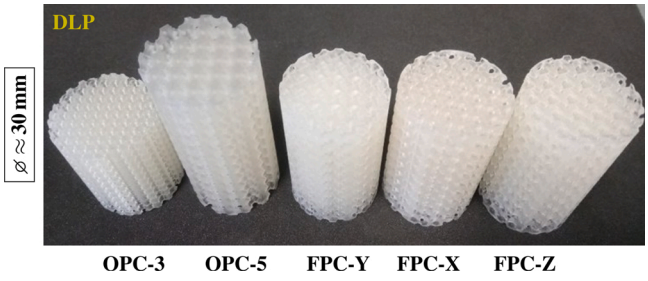

Fig. C.3. OPC and FPC samples ($\phi \approx 30$ mm) manufactured by MIT from a photopolymer resin.

The OPC and FPC samples ($\phi \approx 30$ mm) manufactured by MIT in DLP technology are shown in Fig. C.3. Their quality was good, comparable with the high quality of resin samples manufactured in SLA technology by UTC, EMPA, and TCD.

The top faces of OPC and FPC samples ($\phi \approx 40$ mm) produced by TUe in FFF technology are shown in Fig. C.4. The surface of these samples is moderately uneven, but without fibres, however the shape mapping is rather rough. Their overall quality is estimated to be lower than that of the samples manufactured with *Flashforge Creator PRO* or *Zortrax M200*, comparable to the quality of the samples manufactured with *Creality Ender 3*, and higher than the quality of the samples manufactured with *Makerbot Replicator Z18*.

Appendix D. Impedance tube setup

Fig. D.1 shows a typical configuration used for acoustic testing of 3D printed samples. The setup consists of a round impedance tube with two high-quality microphones (in "the middle") and a loudspeaker at one end of the tube. The sample is inserted at the other end and the tube is sealed with a rigid piston. In some tests an air gap of 40 mm was left between the rigid piston and the bottom of the sample. The microphones are fixed at a certain distance from the sample surface and the distance between them depends on the diameter of the tube. The white noise signal is sent to the loudspeaker by a signal generator usually via an amplifier. The pressure signals measured by the microphones are sent to a multi-channel analyser (i.e. data acquisition hardware) operated by means of a signal analysing software according to the two-microphone transfer function method [44]. Fig. D.1 shows the *Brüel&Kjær* impedance tube kit ($\phi = 29$ mm) used by IPPT, equipped with two *B&K* quarter-inch pressure-field microphones (Type 4187) and a 6-channel module of *B&K* LAN-XI data acquisition hardware (Type 3050-A-060); the signal generator was Arbitrary Waveform Generator *Rigol* DG1022.

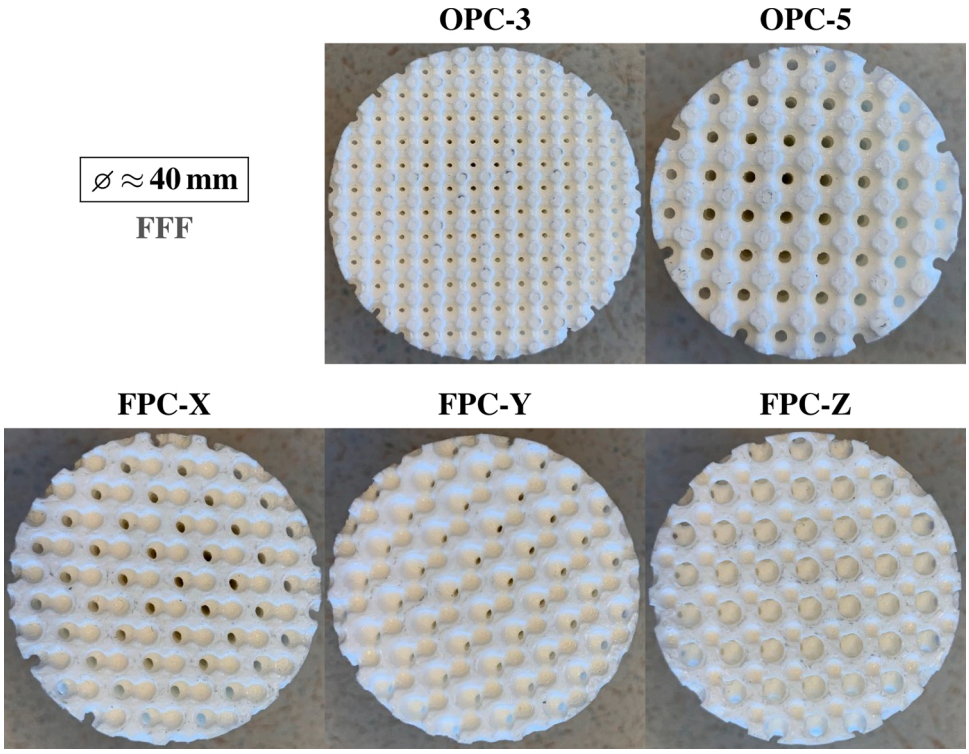

Fig. C.4. OPC and FPC samples ($\phi \approx 40$ mm) manufactured by TUe from ABS polymer filament.

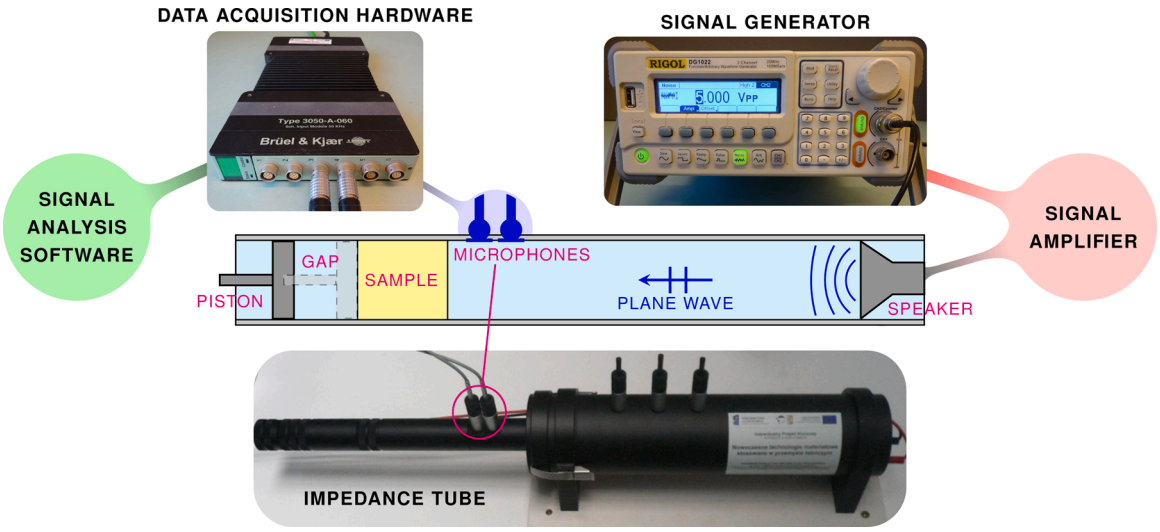

Fig. D.1. Impedance tube measurement kit.

Appendix E. Surface acoustic impedance for some of the FPC samples

Figs. E.1, E.2, E.3 show the real and imaginary parts of the (normalized) surface acoustic impedance measured for some FPC samples. The surface acoustic impedance shown on the graphs is normalized, i.e. divided by the characteristic air impedance accurately determined during the acoustic tests on the basis of ambient mean pressure, temperature, and humidity conditions.

The impedance curves were measured in 29 mm tubes by sample manufacturers and independently by ECL. In fact, they were used to calculate the corresponding sound absorption curves, which are presented in Section 5.2. One may notice that the poles (zeroes) of the imaginary part of the surface impedance correspond to the extrema (local minima and maxima) of its real part, and to the extrema (but this time local maxima and minima, respectively) of the corresponding absorption curve. We present these impedance curves because they can be useful when looking for discrepancies, since in absorption curves some of the measured information is "compacted". The impedance curves measured for different samples of the same (macro- and) micro-geometry are still very similar but perhaps with more noticeable discrepancies. Finally, it should be noted again that the results measured by IPPT and ECL for the same sample are practically the same or very similar, although the tests were carried out in different laboratories over a period of several months (in early springtime by IPPT, and in summertime by ECL).

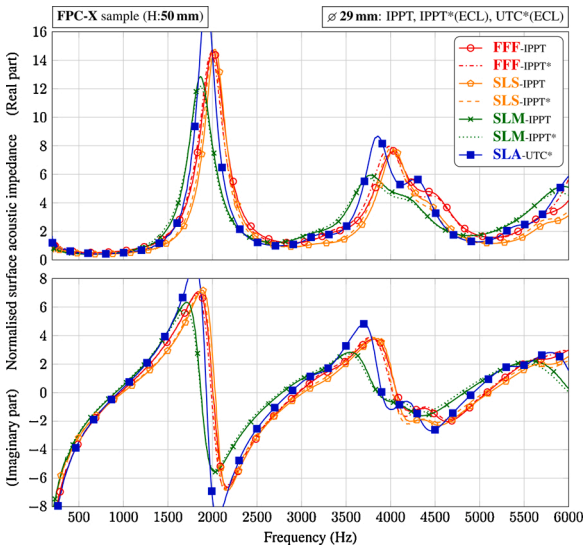

Fig. E.1. Normalized surface acoustic impedance independently measured by ECL and IPPT for some FPC-X samples manufactured by IPPT and UTC.

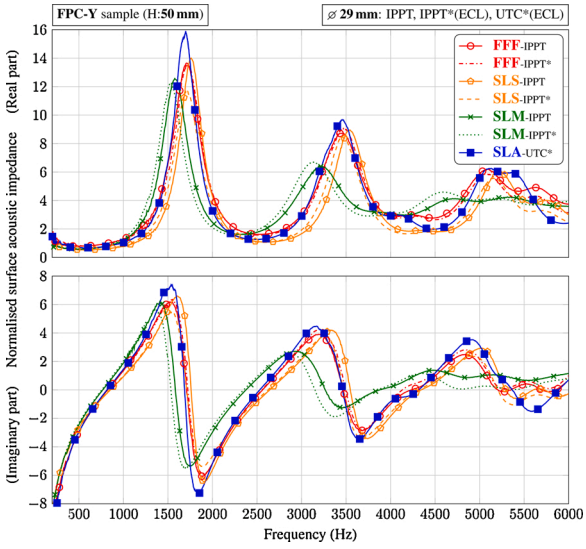

Fig. E.2. Normalized surface acoustic impedance independently measured by ECL and IPPT for some FPC-Y samples manufactured by IPPT and UTC.

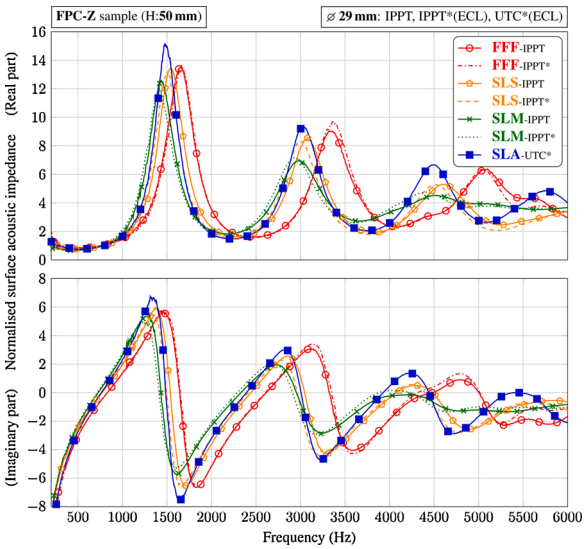

Fig. E.3. Normalized surface acoustic impedance independently measured by ECL and IPPT for some FPC-Z samples manufactured by IPPT and UTC.

Appendix F. Supplementary data

Supplementary data associated with this article can be found, in the online version, at https://doi.org/10.1016/j.addma.2020.101564.

References

[1] J.F. Allard, N. Atalla, Propagation of Sound in Porous Media: Modeling Sound Absorbing Materials, 2nd ed., John Wiley & Sons, Chichester, 2009.
[2] J. Boulvert, T. Cavalieri, J. Costa-Baptista, L. Schwan, V. Romero-García, G. Gabard, E.R. Fotsing, A. Ross, J. Mardjono, J.-P. Groby, Optimally graded porous material for broadband perfect absorption of sound, J. Appl. Phys. 126 (2019) 175101.
[3] K. Attenborough, Microstructures for lowering the quarter wavelength resonance frequency of a hard-backed rigid-porous layer, Appl. Acoust. 130 (2018) 188–194.
[4] K. Attenborough, Macro- and micro-structure designs for porous sound absorbers, Appl. Acoust. 145 (2019) 349–357.
[5] I. Gibson, D. Rosen, B. Stucker, Additive Manufacturing Technologies: 3D Printing, Rapid Prototyping, and Direct Digital Manufacturing, 2nd ed., Springer-Verlag, New York, 2015.
[6] S. Kumar, A.K.S. Choudhary, A.K. Singh, A.K. Gupta, A comparison of additive manufacturing technologies, Int. J. Innov. Res. Sci. Technol. 3 (2016) 147–152.
[7] T.D. Ngo, A. Kashani, G. Imbalzano, K.T. Nguyen, D. Hui, Additive manufacturing (3D printing): a review of materials, methods, applications and challenges, Compos. Part B-Eng. 143 (2018) 172–196.
[8] X. Wang, M. Jiang, Z. Zhou, J. Gou, D. Hui, 3D printing of polymer matrix composites: a review and prospective, Compos. Part B-Eng. 110 (2017) 442–458.
[9] A. Mitchell, U. Lafont, M. Hołyńska, C. Semprimoschnig, Additive manufacturing – a review of 4D printing and future applications, Addit. Manuf. 24 (2018) 606–626.
[10] O. Diegel, A. Nordin, D. Motte, A Practical Guide to Design for Additive Manufacturing, 1st ed., Springer, Singapore, 2019. Springer Series in Advanced Manufacturing.
[11] M. Jiménez, L. Romero, I.A. Domínguez, M.d.M. Espinosa, M. Domínguez, Additive manufacturing technologies: an overview about 3D printing methods and future prospects, Complexity 2019 (2019) 9656938.
[12] ISO 17296-2, Additive Manufacturing – General Principles – Part 2: Overview of Process Categories and Feedstock, 2015.
[13] T.G. Zieliński, Pore-size effects in sound absorbing foams with periodic microstructure: modelling and experimental verification using 3D printed

specimens, in: P. Sas, D. Moens, A. van de Walle (Eds.), Proceedings of ISMA2016 International Conference on Noise and Vibration Engineering and USD2016 International Conference on Uncertainty in Structural Dynamics, 2016, pp. 95–104.
[14] K.C. Opiela, T.G. Zieliński, Microstructural design, manufacturing and modelling of an adaptable porous composite sound absorber, Compos. Part B-Eng. 187 (2020) 107833.
[15] H.J. Rice, J. Kennedy, P. Göransson, L. Dowling, D. Trimble, Design of a Kelvin cell acoustic metamaterial, J. Sound Vib. 472 (2020) 115167.
[16] J. Boulvert, J. Costa-Baptista, T. Cavalieri, M. Perna, E.R. Fotsing, V. Romero-García b, G. Gabard, A. Ross, J. Mardjono, J.-P. Groby, Acoustic modeling of micro-lattices obtained by additive manufacturing, Appl. Acoust. 164 (2020) 107244.
[17] L. Astolfi, R.L. Watson, D.A. Hutchins, P.J. Thomas, M. Askari, A.T. Clare, L. Nie, S. Freear, S. Laureti, M. Ricci, Negative refraction in conventional and additively manufactured phononic crystals, 2019 IEEE International Ultrasonics Symposium (IUS) (2019) 2529–2532.
[18] E.R. Fotsing, A. Dubourg, A. Ross, J. Mardjono, Acoustic properties of periodic micro-structures obtained by additive manufacturing, Appl. Acoust. 148 (2019) 322–331.
[19] T. Ring, S. Langer, Design, experimental and numerical characterization of 3D-printed porous absorbers, Materials 12 (2019) 3397.
[20] Z. Liu, J. Zhan, M. Fard, J. Davy, Acoustic properties of multilayer sound absorbers with a 3D printed micro-perforated panel, Appl. Acoust. 121 (2017) 25–32.
[21] Z. Liu, J. Zhan, M. Fard, J. Davy, Acoustic measurement of a 3D printed micro-perforated panel combined with a porous material, Measurement 104 (2017) 233–236.
[22] T.G. Zieliński, F. Chevillotte, E. Deckers, Sound absorption of plates with micro-slits backed with air cavities: analytical estimations, numerical calculations and experimental validations, Appl. Acoust. 146 (2019) 261–279.
[23] K.V. Horoshenkov, A. Khan, F.-X. Bécot, L. Jaouen, F. Sgard, A. Renault, N. Amirouche, F. Pompoli, N. Prodi, P. Bonfiglio, G. Pispola, F. Asdrubali, J. Hübelt, N. Atalla, C.K. Amédin, W. Lauriks, L. Boeckx, Reproducibility experiments on measuring acoustical properties of rigid-frame porous media (round-robin tests), J. Acoust. Soc. Am. 122 (2007) 345–353.
[24] P. Bonfiglio, F. Pompoli, K.V. Horoshenkov, M.I.B.S.A. Rahim, L. Jaouen, J. Rodenas, F.-X. Bécot, E. Gourdon, D. Jaeger, V. Kursch, M. Tarello, N.B. Roozen, C. Glorieux, F. Ferrian, P. Leroy, F.B. Vangosa, N. Dauchez, F. Foucart, L. Lei, K. Carillo, O. Doutres, F. Sgard, R. Panneton, K. Verdiere, C. Bertolini, R. Bär, J.-P. Groby, A. Geslain, N. Poulain, L. Rouleau, A. Guinault, H. Ahmadi, C. Forge, How reproducible are methods to measure the dynamic viscoelastic properties of poroelastic media? J. Sound Vib. 428 (2018) 26–43.
[25] A. du Plessis, S.G. le Roux, Standardized X-ray tomography testing of additively manufactured parts: a round robin test, Addit. Manuf. 24 (2018) 125–136.
[26] A. Townsend, R. Racasan, R. Leach, N. Senin, A. Thompson, A. Ramsey, D. Bate, P. Woolliams, S. Brown, L. Blunt, An interlaboratory comparison of X-ray computed tomography measurement for texture and dimensional characterisation of additively manufactured parts, Addit. Manuf. 23 (2018) 422–432.
[27] A. du Plessis, S.G. le Roux, J. Waller, P. Sperling, N. Achilles, A. Beerlink, J.-F. Métayer, M. Sinico, G. Probst, W. Dewulf, F. Bittner, H.-J. Endres, M. Willner, Á. Drégelyi-Kiss, T. Zikmund, J. Laznovsky, J. Kaiser, P. Pinter, S. Dietrich, E. Lopez, O. Fitzek, P. Konrad, Laboratory X-ray tomography for metal additive manufacturing: round robin test, Addit. Manuf. 30 (2019) 100837.
[28] J. Kennedy, L. Flanagan, L. Dowling, G.J. Bennett, H. Rice, D. Trimble, The influence of additive manufacturing processes on the performance of a periodic acoustic metamaterial, Int. J. Polym. Sci. 2019 (2019) 7029143.
[29] T.G. Zieliński, K.C. Opiela, P. Pawłowski, N. Dauchez, T. Boutin, J. Kennedy, D. Trimble, H. Rice, Differences in sound absorption of samples with periodic porosity produced using various Additive Manufacturing Technologies, in: M. Ochmann, M. Vorländer, J. Fels (Eds.), Proceedings of the 23rd International Congress on Acoustics integrating 4th EAA Euroregio 2019, Deutsche Gesellschaft für Akustik, 2019, pp. 1216–1223.
[30] T.G. Zieliński, R. Venegas, C. Perrot, M. Červenka, F. Chevillotte, K. Attenborough, Benchmarks for microstructure-based modelling of sound absorbing rigid-frame porous media, J. Sound Vib. 483 (2020) 115441.
[31] J.-P. Dalmont, Acoustic impedance measurement. Part I. A review, J. Sound Vib. 243 (2001) 427–439.
[32] J.-P. Dalmont, Acoustic impedance measurement. Part II. A new calibration method, J. Sound Vib. 243 (2001) 441–459.
[33] R. Boonen, P. Sas, W. Desmet, W. Lauriks, G. Vermeir, Calibration of the two microphone transfer function method with hard wall impedance measurements at different reference sections, Mech. Syst. Signal. Process. 23 (2009) 1662–1671.
[34] T.G. Zieliński, Generation of random microstructures and prediction of sound velocity and absorption for open foams with spherical pores, J. Acoust. Soc. Am. 137 (2015) 1790–1801.
[35] J.A. García Galicia, B. Benes, Improving printing orientation for Fused Deposition Modeling printers by analyzing connected components, Addit. Manuf. 22 (2018) 720–728.
[36] B. Ghanbarian, A.G. Hunt, R.P. Ewing, M. Sahimi, Tortuosity in porous media: a critical review, Soil Sci. Soc. Am. J. 77 (2013) 1461–1477.
[37] P.C. Carman, Fluid flow through granular beds, Trans. Inst. Chem. Eng. Lond. 15 (1937) 150–166. Reprinted in: Chem. Eng. Res. Des. 75 Suppl. (1997) S32–S48.
[38] J. Bear, Dynamics of Fluids in Porous Media, Dover Publ., New York, 1988.
[39] D.L. Johnson, J. Koplik, R. Dashen, Theory of dynamic permeability and tortuosity in fluid-saturated porous media, J. Fluid Mech. 176 (1987) 379–402.
[40] Y. Champoux, J.F. Allard, Dynamic tortuosity and bulk modulus in air-saturated porous media, J. Appl. Phys. 70 (1991) 1975–1979.
[41] D. Lafarge, P. Lemarinier, J.F. Allard, V. Tarnow, Dynamic compressibility of air in porous structures at audible frequencies, J. Acoust. Soc. Am. 102 (1997) 1995–2006.
[42] L. Yang, K. Hsu, B. Baughman, D. Godfrey, F. Medina, M. Menon, S. Wiener, Additive manufacturing of metals: the technology, materials, design and production, 1st ed., Springer International Publishing, 2017. Springer Series in Advanced Manufacturing.
[43] L. Dowling, J. Kennedy, S. O'Shaughnessy, D. Trimble, A review of critical repeatability and reproducibility issues in powder bed fusion, Mater. Des. 186 (2020) 108346.
[44] ISO 10534-2 Determination of Sound Absorption Coefficient and Impedance in Impedance Tubes, 1998.
[45] ASTM E1050-19: Standard Test Method for Impedance and Absorption of Acoustical Materials Using A Tube, Two Microphones and A Digital Frequency Analysis System, 2019.
[46] A. du Plessis, Effects of process parameters on porosity in laser powder bed fusion revealed by X-ray tomography, Addit. Manuf. 30 (2019) 100871.
[47] R.J. Williams, A. Piglione, T. Rønneberg, C. Jones, M.-S. Pham, C.M. Davies, P. A. Hooper, In situ thermography for laser powder bed fusion: effects of layer temperature on porosity, microstructure and mechanical properties, Addit. Manuf. 30 (2019) 100880.
[48] A. Cummings, Impedance tube measurements on porous media: the effects of air-gaps around the sample, J. Sound Vib. 151 (1991) 63–75.
[49] Y. Ibrahim, Z. Li, C.M. Davies, C. Maharaj, J.P. Dear, P.A. Hooper, Acoustic resonance testing of additive manufactured lattice structures, Addit. Manuf. 24 (2018) 566–576.
[50] OpenSCAD – The Programmers Solid 3D CAD Modeller. https://www.openscad.org/ (Last viewed 18 February 2020).
[51] OpenSCAD Language. https://en.wikibooks.org/wiki/OpenSCAD_User_Manual/The_OpenSCAD_Language (Last viewed 18 February 2020).
[52] FreeCAD – Open-Source 3D Parametric CAD Modeler. https://www.freecadweb.org/ (Last viewed 18 February 2020).
[53] Import OpenSCAD Code (in FreeCAD). https://www.freecadweb.org/wiki/Import_OpenSCAD_code (Last viewed 18 February 2020).